

# Global Biogeochemical Cycles

## RESEARCH ARTICLE

10.1029/2020GB006772

### Key Points:

- Soil organic carbon density is lower in the Chinese unvegetated tidal flats than vegetated coastal area in the world
- The overall carbon sequestration rate of Chinese tidal flats is comparable to rates of global coastal marshes
- Tidal flats account for nearly 80% of the C stored in the Chinese tidal area

### Supporting Information:

- Supporting Information S1

### Correspondence to:

D. Wang,  
dqwang@geo.ecnu.edu.cn

### Citation:





Chen, J., Wang, D., Li, Y., Yu, Z., Chen, S., Hou, X., et al. (2020). The carbon stock and sequestration rate in tidal flats from coastal China. *Global Biogeochemical Cycles*, 34, e2020GB006772. <https://doi.org/10.1029/2020GB006772>

Received 30 JUL 2020

Accepted 6 NOV 2020

Accepted article online 17 NOV 2020

## The Carbon Stock and Sequestration Rate in Tidal Flats From Coastal China

Jie Chen<sup>1,2</sup> , Dongqi Wang<sup>1,3</sup> , Yangjie Li<sup>4</sup>, Zhongjie Yu<sup>5</sup>, Shu Chen<sup>1,3</sup> , Xiyong Hou<sup>6,7</sup>, John R. White<sup>8</sup> , and Zhenlou Chen<sup>1,3</sup>

<sup>1</sup>Key Laboratory of Geographic Information Science (Ministry of Education), East China Normal University, Shanghai, China, <sup>2</sup>School of Ecological and Environmental Sciences, East China Normal University, Shanghai, China, <sup>3</sup>School of Geographic Sciences, East China Normal University, Shanghai, China, <sup>4</sup>Key Laboratory of Marine Ecosystem and Biogeochemistry, Second Institute of Oceanography, Ministry of Natural Resources, Hangzhou, China, <sup>5</sup>Department of Natural Resources and Environmental Sciences, University of Illinois Urbana-Champaign, Urbana, IL, USA, <sup>6</sup>Yantai Institute of Coastal Zone Research, Chinese Academy of Sciences, Yantai, China, <sup>7</sup>Key Laboratory of Coastal Environmental Processes and Ecological Remediation, Chinese Academy of Sciences, Yantai, China, <sup>8</sup>Department of Oceanography and Coastal Sciences, College of the Coast and Environment, Louisiana State University, Baton Rouge LA, USA

**Abstract** Tidal flats form around the estuarine and coastal zone by continuous terrigenous sediment transport and deposition processes. Now a large body of published carbon research work frame within the vegetated area (mangrove forests, sea grass bed, and salt marshes). Nonvegetated tidal flats, which are characterized by predominantly silts and clays sediment, were generally impressed with low carbon stock due to their meager primary productivity. However, these regions may be a potentially important carbon sink, given their high burial rate, expanding areal coverage, and detrial organic carbon derived from watershed and adjacent vegetated area. Low carbon densities ( $<0.01 \text{ g cm}^{-3}$ ) were found in Chinese tidal flat sediments by the study, but the carbon sequestration rates ranged from 35 to 361  $\text{g C m}^{-2} \text{ yr}^{-1}$ , which were comparable to rates of worldwide vegetated coastal areas. The high rates can be ascribed to rapid sedimentation rates ( $1\text{--}2 \text{ cm yr}^{-1}$ ) during the past several decades. The highest areal carbon stocks were located at tidal flat sites proximal to mangrove forests. The majority of carbon stocks (100 cm) was found in the unvegetated tidal flats instead of in the vegetated tidal flats. The former occupied 87% of the entire tidal area, 6.7 times larger than the latter. Tidal flats in coastal China store 78.07 Tg C (100 cm), accounting for nearly 80% of the C deposited in entire coastal tidal area. The future carbon sequestration rates of Chinese tidal flats are facing uncertainties under the pressures of reduced fluvial sediment loads from major rivers.

## 1. Introduction

Vegetated coastal areas, such as marshes, mangrove forests, and seagrass, cover  $<2\%$  of the ocean surface but contribute to about 50% of all the organic carbon burial in the ocean sediments (Duarte et al., 2005). The global carbon burial rate of coastal vegetated areas has been reported to range from 114 to 131 Tg C  $\text{yr}^{-1}$  (Nellemann et al., 2009). Many factors influence carbon burial rate, including vegetation type and coverage, allochthonous sediment inputs, sedimentation rates, decomposition rates, bioturbation, and other hydrometeorology factors (Perillo et al., 2009). Some studies indicate that about 70% of organic carbon transported by rivers is oxidized in the continental margin, leaving the overall burial efficiency of organic carbon at 30%, except in areas with very high sedimentation rates (i.e., the Bengal fan) (Burdige, 2005; Galy et al., 2007). In general, organic carbon delivered by rivers to deltaic intertidal wetlands is deemed relatively refractory (i.e., resistant to in situ decomposition) (Dodla et al., 2012), while organic carbon from marine sources is generally more readily decomposed (Burdige, 2005). Regardless of carbon source, the sedimentation rate is an essential determinant of carbon burial rates in the coastal systems (Chmura et al., 2003). Greater organic carbon is preserved under high sedimentation rates found in the Mississippi River delta, Amazon delta, Yangtze delta, and Fly delta (Aller, 1998, and references therein). The flooded soil condition and low oxygen status of coastal area soils lead to greater preservation of buried carbon over time. Coastal wetlands are highly efficient carbon sinks; the mean carbon sequestration rates of salt marshes and mangroves are  $2.18 \pm 0.24$

and  $2.26 \pm 0.39 \text{ Mg C ha}^{-1} \text{ yr}^{-1}$  (mean  $\pm$  SE), respectively (Mcleod et al., 2011), much higher than cropland ecosystems (West & Post, 2002).

Broad tidal flats characterized predominantly with silts and clays can be defined as a muddy coast (Wang et al., 2002). Previously, mud flats, salt marshes, and mangrove swamps with or without vegetation were all classified as tidal flats (Flemming, 2002). Here, the study focusses on nonvegetated tidal flats, which are fringed by marsh and mangroves and also exist as the form of exclusive barren surface. In contrast to the well-studied marshes and mangrove systems, the global distribution of tidal flats had not been mapped until recently (Murray et al., 2019a). However, carbon sequestration rates for these areas remain relatively unknown (Gorma et al., 2020; Perillo et al., 2009). Meng et al. (2019) reviewed the published data and found a total of 48.12–123.95 Tg C (100 cm) stock in China's coastal vegetated wetlands. Additionally, Fu et al. (2020) reported that Chinese mangrove, salt marsh, and seagrass habitats stored 15.4 Tg C (100 cm). Lack of unified field sampling and lab analysis methods contribute above large gaps of the carbon stock. Currently, it seems that there is no systematic field research about unvegetated tidal flats at national wide level. Regional studies have found that an average C density in Gulf of Mexico marshes was  $0.052 \text{ g cm}^{-3}$ , an order of magnitude larger than the C density in mudflats of the Wadden Sea (Chmura et al., 2003; Postma, 1981; Volkman et al., 2000). Rapid sedimentation rates can promote burial of OC in tidal mudflat associated with a major riverine sediment source (Choi & Wang, 2004). Tidal flats, located in deltaic regions, receive high concentrations of suspended sediment and also could experience high C sequestration rate due to rapid burial rate (Roberts et al., 2015).

Tidal flats are one of the dominant habitats along the Chinese coast. This is especially true for northern China where the alluvial plain has prograded seaward over the past thousands of years due to high sediment transport of large river systems (Wang, 1983). Currently, the suspended sediment loads of major rivers are much less than the loads in the twentieth century due to construction of dams and application of soil erosion control measures (Wang et al., 2007, 2016; Xu & Milliman, 2009; Yang et al., 2007). Decreased river sediment loads create an uncertain future for C sequestration of associated coastal systems. At the same time, the Chinese coastal region has experienced large reclamation activities and sea defenses construction (Ma et al., 2014; Paulson Institute et al., 2015), which may impact carbon stock and sequestration rates in these wetlands. Many previous studies of Chinese coastal wetlands have focused on the supratidal zones or adjacent areas proximal to the high spring tidal watermark (Bai et al., 2012; Duan et al., 2008; Liu et al., 2007; Zhang et al., 2010), perhaps due, in part to accessibility issues related to navigating soft muds. This research incorporated the organic C content, bulk density, accretion rates, C sequestration rate, and C stock in the research plan of a number of tidal flats along the Chinese coastline. All these tidal flats are outside of seawall and experience semidiurnal or diurnal tide.

## 2. Material and Methods

### 2.1. Study Sites

Twelve sampling sites were selected, namely, LiaoHe (LH), HanGu (HG), DongYing (DY), QingDao (QD), YanCheng (YC), DongTan (DT), CiXi (CX), FuZhou (FZ), JiuLong (JL), ZhuJiang (ZJ), DongZhai (DZ), and YingLuo (YL) (Figure 1). Several essential parameters, including tidal flat type, tidal type and range, average annual and monthly temperature range, salinity, and mean annual precipitation, were summarized in Table S1 in the supporting information. All these tidal flats are outside of the constructed seawalls and are inundated by spring tides. All study sites are under the influence of the East Asian monsoon climate, which is characterized by warm wet summers and cold dry winters. The sites located south of  $31^\circ\text{N}$  are also influenced by the occasional tropical cyclones, which impact the coastline during the summer and autumn seasons. The wetland type of each study site was classified based on the Ramsar classification system (Table S1) (Ramsar Convention Secretariat, 2013).

### 2.2. Sediment Collection

The sampling was carried out through two phases, one set of sites was sampled in the winter of 2014 and the other was sampled in the following summer. At each site, the sampling depth was 15 cm. For the winter sampling, five transects were established at each site, and each transect was divided into high, middle, and low regions based upon the bathymetry and inundation frequency by spring and neap tides. The summer

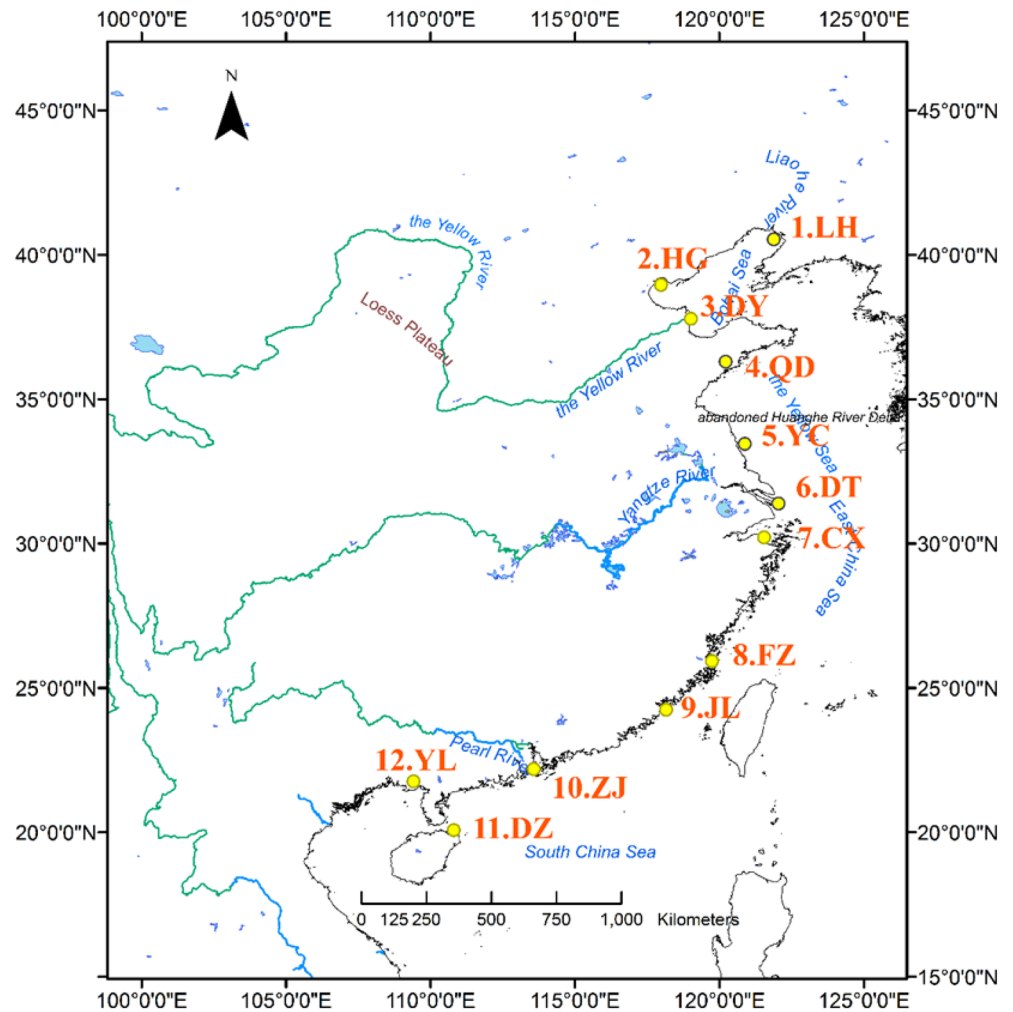


**Figure 1.** Map of the sampling sites, 12 tidal flats sites on the coast of east China. From the north to the south, they are the mouth of Liaohu River (LH), Tianjin Hangu (HG), the mouth of Yellow River (DY), Jiaozhou Bay of Qingdao (QD), Yancheng (YC), Chongming Dongtan (DT), Cixi (CX), the mouth of Minjiang River in Fuzhou (FZ), the mouth of Jiulong River (JL), the mouth of Pearl River (ZJ), Dongzhai Port (DZ), and Yingluo Bay (YL).

sampling event revisited the five transects previously sampled in the winter and added an additional 10 transects for each site. In total, 720 surficial samples were collected. The samples were stored frozen at  $-18^{\circ}\text{C}$  before analyses.

Twenty-six sediment cores (10 cm diameter and 110 cm long) were collected by using cylindrical polymethyl methacrylate tubes at 12 sampling sites from September to the end of 2014. Duplicate cores were taken at each site, except at LH and YC where triplicate cores were collected. The cores were immediately sealed with rubber stoppers, transported back to the laboratory, and stored at  $4^{\circ}\text{C}$  prior to analysis.

### 2.3. Sediment Analysis

Sediment cores were sectioned at 2-cm intervals weighed, and then each section was subdivided to form four subsamples that were dried at  $70^{\circ}\text{C}$  for 48 h to allow for calculation of dry bulk density and water content. The samples were subsequently ground for analysis of grain size (Mastersizer 2000, Malvern). Given the wide distribution of calcareous soils in northern China (Mi et al., 2008), this study employed the heated dichromate method (tube digestion method), which decomposed organic carbon completely and does not require a correction factor for inorganic carbon (Nelson & Sommers, 1996). Total C content of sediments were determined by the elemental analyzer (vario MICRO cube, Elementar GmbH). The results were verified and calibrated by standard reference materials. The recovery of these standards was  $98.5\% \pm 0.6\%$ . Inorganic carbon content was the result of subtracting organic carbon from total carbon.

Activities of  $^{210}\text{Pb}$ ,  $^{214}\text{Pb}$ , and  $^{137}\text{Cs}$  were measured simultaneously using four high-purity Germanium well  $\gamma$  ray detectors (ORTEC GWL-120-15, AMETEK). After a 20-day equilibrium period, activities of  $^{214}\text{Pb}$  and total  $^{210}\text{Pb}$  were quantified using 352- and 46.5-keV photopeaks, respectively (Joshi, 1987), and activity of  $^{137}\text{Cs}$  was quantified from counts of 662-keV photopeaks. Unsupported  $^{210}\text{Pb}$  activities were derived from subtraction of supported  $^{210}\text{Pb}$  activities from the total  $^{210}\text{Pb}$  activities (Joshi, 1987).

#### 2.4. Calculation of Carbon Stocks, Density, and Sedimentation Rates

Carbon stock ( $S_c$ , Mg C  $\text{ha}^{-1}$ ) of each core (100 cm) was calculated as

$$S_c = \sum_{i=1}^n c_n \times \rho_n \times 2 \quad (1)$$

where  $\rho_n$  (Mg  $\text{m}^{-3}$ ) is bulk density and  $C_n$  (mass %) is C concentration of the sample. The value 2 is indicative of the length of sample section, 2 cm.

Carbon density ( $D_c$ ) of surficial sediment was calculated as

$$D_c = \bar{c} \times \bar{\rho} \quad (2)$$

where  $\bar{\rho}$  (Mg  $\text{m}^{-3}$ ) is mean bulk density and  $\bar{c}$  (mass %) is mean C concentration of the surficial sample.

The constant rate of  $^{210}\text{Pb}$  supply (also known as constant flux) model (CF) can be applied to nonsteady state sedimentation and nonmonotonic profiles of unsupported  $^{210}\text{Pb}$  (Appleby & Oldfieldz, 1983). Here the study used CF model to elucidate the dates and sediment fluxes of the cores (Nriagu, 1978).

The activity of unsupported  $^{210}\text{Pb}$  is gained by

$$A_m = \frac{f}{G(t)} e^{-\lambda t} \quad (3)$$

where  $A_m$  (Bq  $\text{kg}^{-1}$ ) is the unsupported (excess) activity of  $^{210}\text{Pb}$  at depth  $m$ .  $G(t)$  ( $\text{kg cm}^{-2} \text{yr}^{-1}$ ) is the sedimentation mass during the time  $t$ ; alternatively, it can convey as  $G(t) = dm/dt$ .  $\lambda$  ( $0.0311 \text{yr}^{-1}$ ) is the radioactive decay constant for  $^{210}\text{Pb}$ . Variable  $f$  ( $\text{Bq cm}^{-2} \text{yr}^{-1}$ ) is the constant supply rate of unsupported  $^{210}\text{Pb}$ , so it can express as

$$f = \lambda \int_0^\infty A_m dm \quad (4)$$

Then Equation 3 is transformed as

$$\int_m^\infty A_m dm = \int_t^\infty f e^{-\lambda t} dt = \frac{f}{\lambda} e^{-\lambda t} = e^{-\lambda t} \int_0^\infty A_m dm \quad (5)$$

Based above equations, the age  $t$  can be deduced as

$$t = \frac{1}{\lambda} \ln \frac{\int_0^\infty A_m dm}{\int_m^\infty A_m dm} \quad (6)$$

And mass flux  $G(t)$  is also gained by using Equations 3 and 5 as the form of

$$G(t) = \frac{f e^{-\lambda t}}{A_m} = \frac{\lambda \int_m^\infty A_m dm}{A_m} \quad (7)$$

Finally, the sequestration rate of soil organic carbon is calculated based above sedimentation rate

$$S_{oc} = G(t) \text{ OC (mass\%)} 10 \quad (8)$$

Among this (Equation 8),  $S_{oc}$  ( $\text{g C m}^{-2} \text{yr}^{-1}$ ) is the organic carbon sequestered per year per square meter. OC is mass percent of organic carbon. The constant 10 is the adjustment factor for the conversion of units. Sedimentation flux rates calculated from above CF model were checked using  $^{137}\text{Cs}$  data.

The study also used a CIC (constant initial concentration) model (Equation 9) to calculate the sedimentation rate ( $\text{cm yr}^{-1}$ ).

$$A_m = A_0 e^{-\lambda t} \quad (9)$$

The  $A_0$  in Equation 9 means the initial unsupported activity of  $^{210}\text{Pb}$ .

### 2.5. The Area of Tidal Flats in China and Estimation of Carbon Stock

Since one of the primary goals of this study is to estimate the carbon stock of Chinese tidal flats, the total areal extent is required. The largest coastline and peritidal zone study was carried out during the 1980s. The results indicated that there were  $\sim 22,000 \text{ km}^2$  of coastal wetlands in China (Ren, 1996), including regions above the high tide level and below the low tide level. The example of Shanghai showed this sum was the merged result based on tidal range and bathymetry (Chen et al., 1988). However, during the past 70 years, nearly  $14,200 \text{ km}^2$  coastal areas have been reclaimed from the sea (Hou et al., 2016). More than 60% of the coastal wetlands along the Chinese coast are surrounded by seawalls (Ma et al., 2014).

Based on 707,528 Landsat images, digital elevation, and bathymetry models, the distribution of global tidal flats (no plant coverage) was mapped by Murray et al. (2019a). The accuracy of above result was 82%, and this provided a reliable estimate on tidal flat coverage, given that multiple validation methods were employed (Murray et al., 2019a). The study used this open data set (Murray et al., 2019b) to determine the Chinese tidal flats area in 2016. We divided Chinese tidal flats into 12 sectors, most of which were separated by the province borders, except for the Yellow River delta and the Jiulong River estuary. The latter two area were extracted independently, as their sediment attributes were not analogous to adjacent tidal regions. The study assumed carbon distribution of each sector to be consistent. Each sampling site represents each specific region except for the Yellow River delta and Jiulong River estuary.

## 3. Results

### 3.1. Sediment Deposition Rates of Tidal Flats

The sedimentation rates based on CIC and  $^{137}\text{Cs}$  ranged from  $0.84$  to  $2.82 \text{ cm yr}^{-1}$  (Table 1). The lowest and highest sedimentation rates occurred in JL and HG, respectively. Except for the extreme values, the sedimentation rate of most tidal flats in China was about  $1\text{--}2 \text{ cm yr}^{-1}$ . The study found three sites, namely, YC, FZ, and YL, for which we could not utilize either CIC, CF models or  $^{37}\text{Cs}$  dating, owing to irregular activities of  $^{210}\text{Pb}$ ,  $^{214}\text{Pb}$ , and  $^{137}\text{Cs}$ , sediment disturbance/reworking, or isotope diffusion (Table 1). The sediments down to  $55 \text{ cm}$  have been deposited since 1960, except for LH01 and JL01 (Figure 2). The top  $20\text{-cm}$  deposition of all the tidal flat cores occurred after the year of 1995 except for LH01 (Figure 2). The rapid sedimentation rates after 1990 occurred in all tidal flats sites, and the sedimentation rates of HG01, QD02, DTS, and JL02 were about 2 times larger than the previous sedimentation rates during 1950–1990 (Table 1). The sediment accretion measurements identified that the sedimentation rates increased abruptly in specified years (Figure 3). The high sedimentation rates at the estuarine sites were closely linked with recorded major or record flooding levels in the river drainage basin, for example, at LH site during 1945 and 1960 (Ministry of Water Resources Songliao River Water Resources Commission, 2002). The abrupt sedimentation rate increments in 1959, 1981, and 1994 at ZJ01 corresponded to the floods in the Pearl River (Zhujiang) (Ministry of Water Resources Pearl River Water Resources Commission, 1994). However, not all sharp changes in sedimentation were related to river flood events. The sedimentation increases in DT and CX were influenced by land reclamation. The sedimentation rate of DT increased dramatically in 1999. The phenomenon was related to large-scale reclamation project launched in 1998 (Gu, 2004). This activity led to a rapid accumulation of mud in front of the seawalls, that is, the high tide zone. Since 1962, a series of land reclamation project initiated at site CX and the most recent seawall was established in 2003 (Zhang, Guo, et al., 2005). All these coastal activities have led to increased sediment accumulation rates in these areas.

### 3.2. Carbon Burial in Sediments From the Yellow River and Yangtze River

The study found no significant difference ( $P > 0.05$ ) between summer and winter samples for sediment organic carbon (SOC) and sediment inorganic carbon (SIC) from the Yellow River and Yangtze River. The

**Table 1**  
The Sedimentation Rate and Organic Carbon Sequestration Rate Based on CIC and CF Model

Samples	Sedimentation status	$^{210}\text{Pb}$ (CIC) (cm yr $^{-1}$ )	$^{137}\text{Cs}$ 1986 (cm yr $^{-1}$ )	$^{137}\text{Cs}$ 1963 (cm yr $^{-1}$ )	C sequestration rate (CIC& $^{137}\text{Cs}$ ) (g C m $^{-2}$ yr $^{-1}$ )	Sedimentation rate 1950–1990(CF) (kg m $^{-2}$ yr $^{-1}$ )	Sedimentation rate 1990–2014(CF) (kg m $^{-2}$ yr $^{-1}$ )	C sequestration rate 1950–1990(CF) (g C m $^{-2}$ yr $^{-1}$ )	C sequestration rate 1990–2014(CF) (g C m $^{-2}$ yr $^{-1}$ )
LH01	Deposition	1.11	—	1.06	64–67	8.20 ± 2.92	11.27 ± 2.12	35.46 ± 17.53	71.59 ± 6.38
LH02	Deposition	1.82	—	1.22	103–154	18.05 ± 11.79	22.47 ± 11.31	103.78 ± 115.23	168.24 ± 63.19
LH03	Deposition	1.00	—	1.33	72–96	20.24 ± 11.29	12.42 ± 2.46	95.88 ± 54.37	82.54 ± 18.55
HG01	Deposition	1.83	—	—	177	8.15 ± 2.79	18.21 ± 5.26	76.08 ± 25.59	158.67 ± 63.26
HG02	Deposition	2.82	2.07	2.08	204–278	15.08 ± 12.08	15.83 ± 2.41	138.40 ± 111.95	133.37 ± 18.33
DY02	Deposition	—	1.57	2	35–46	—	—	—	—
QD02	Deposition	1.72	1.28	1.37	124–166	10.91 ± 3.31	20.26 ± 7.15	85.20 ± 22.74	192.95 ± 77.47
QD03	Deposition	—	1.18	—	98	—	—	—	—
YC01, and YC02, and YC03	Reworking or diffusion	—	—	—	—	—	—	—	—
DT5	Deposition	1.41	—	—	136	11.59 ± 3.26	19.29 ± 4.65	42.68 ± 23.78	91.51 ± 64.84
CX01	Deposition	2.58	—	—	214	13.44 ± 5.43	20.32 ± 5.22	84.12 ± 42.21	153.84 ± 43.56
CX02	Reworking or diffusion	—	—	—	—	—	—	—	—
FZ01 and FZ02	Reworking or diffusion	—	—	—	—	—	—	—	—
JL01	Deposition	0.84	—	—	132	7.05 ± 3.01	11.29 ± 3.17	78.32 ± 43.57	130.66 ± 33.38
JL02	Deposition	0.89	—	—	144	5.14 ± 1.19	10.84 ± 3.26	75.08 ± 20.45	148.10 ± 38.71
ZI01	Deposition	1.24	—	—	126	11.91 ± 3.80	16.85 ± 4.41	54.99 ± 26.78	74.55 ± 62.09
ZI02	Reworking or diffusion	—	—	—	—	—	—	—	—
DZ01	Deposition	1.83	—	—	361	16.95 ± 11.01	17.49 ± 5.38	262.77 ± 176.96	136.63 ± 113.96
DZ02	Reworking or diffusion	—	—	—	—	—	—	—	—
YL01 and YL02	Reworking or diffusion	—	—	—	—	—	—	—	—

Note. Em dash represents data unavailable.

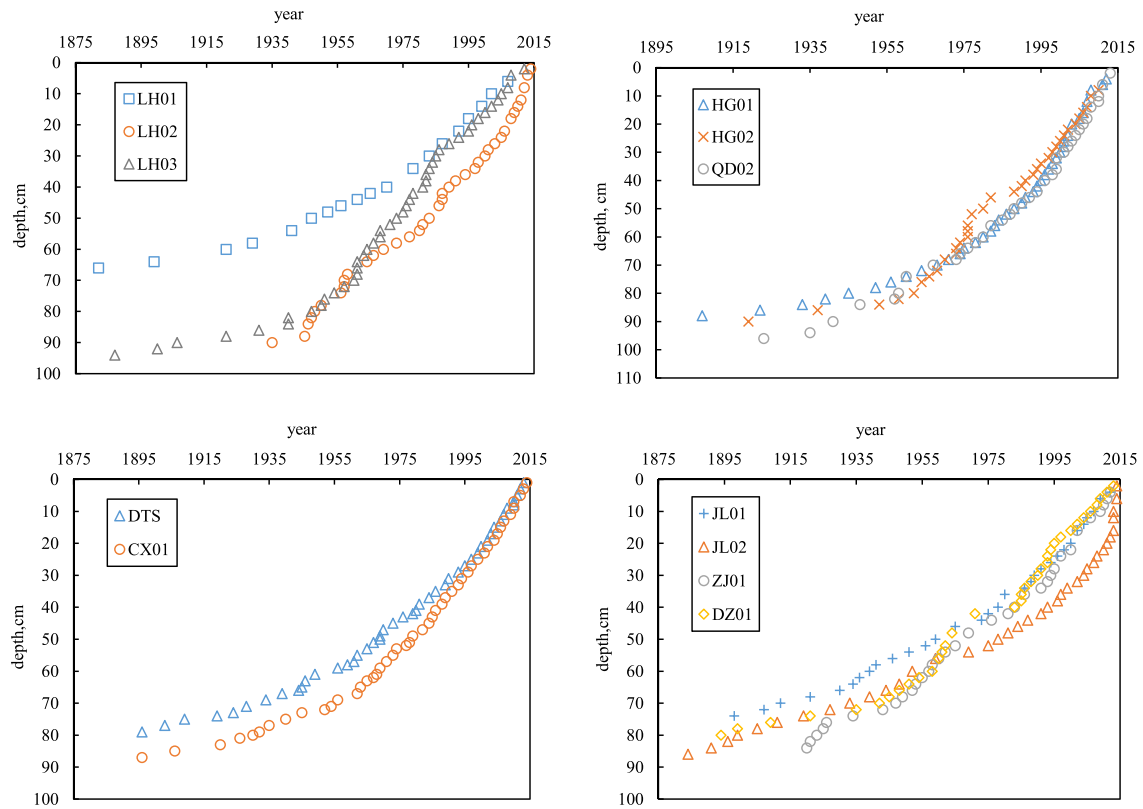


Figure 2. The correlation between sedimentation time and core depth based on CF model.

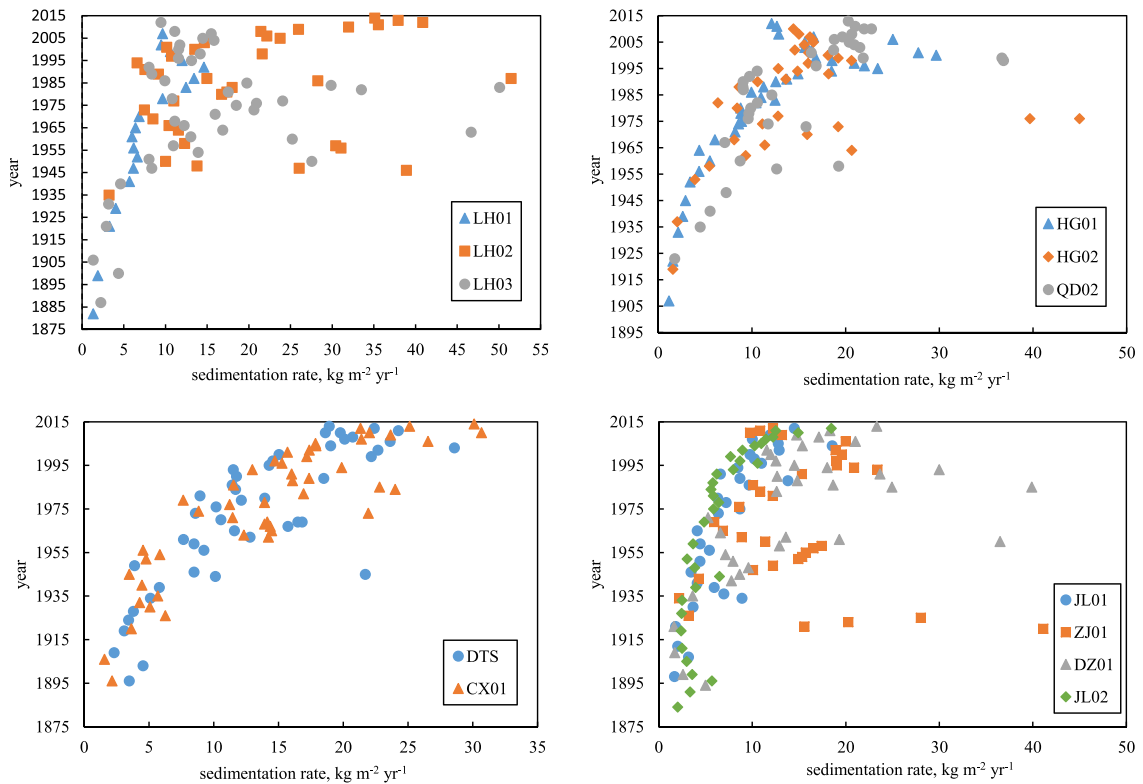
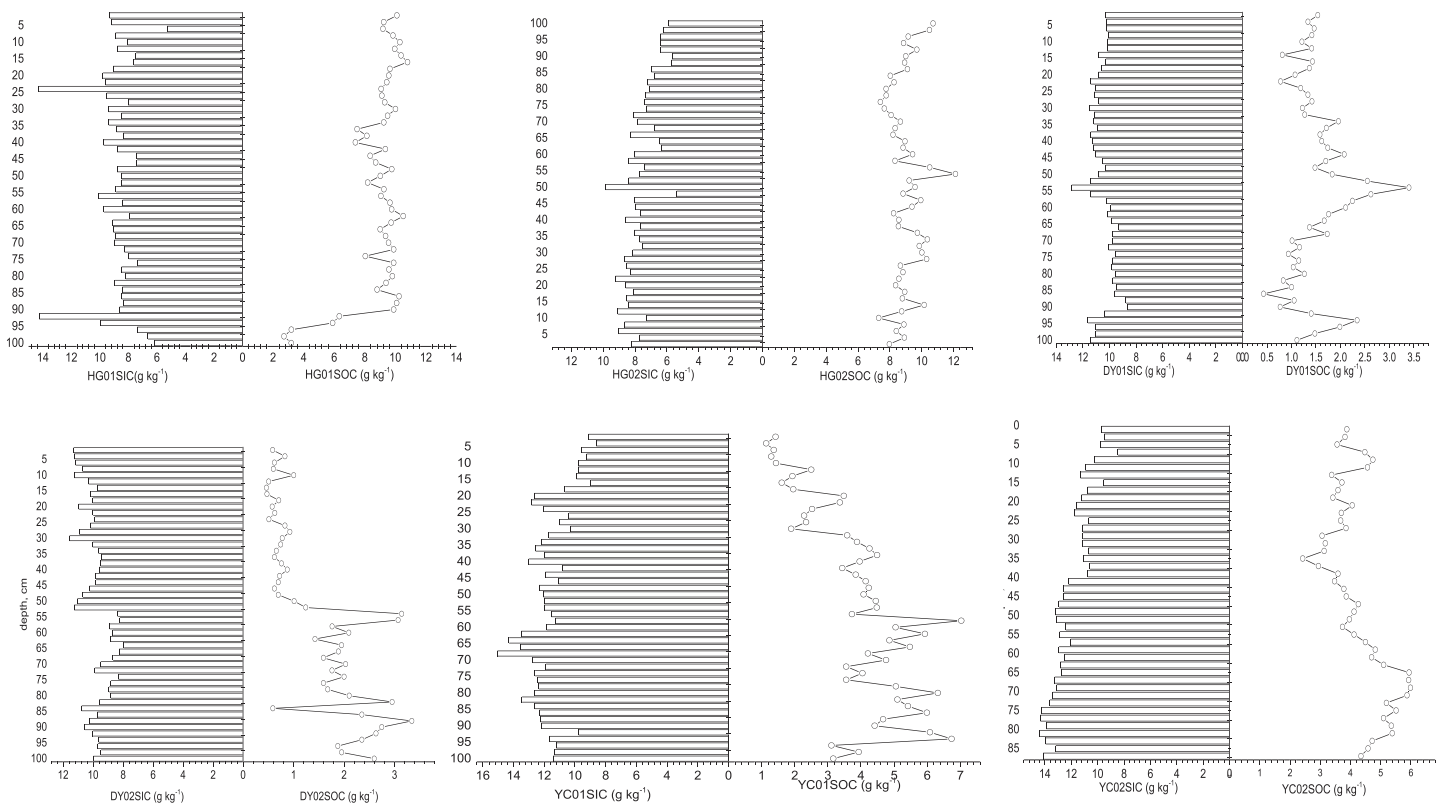


Figure 3. Correlation between sedimentation time and sedimentation rate based on CF model.



**Figure 4.** The SOC and SIC profiles in sites of HG, DY, YC, DT, and CX.

SOC of DY, YC, and DT was generally higher in the high tidal flats than in more seaward positions, denoted as the low tidal flat (Figure S1). There was no difference in SOC at HG between high tidal and low tidal flats, but its lowest SOC was about  $9 \text{ g kg}^{-1}$ . At the high tidal flat of DT, the highest SOC was about  $10 \text{ g kg}^{-1}$ . Much lower surficial SOC covered high and low tidal flats at the DY sites. Another low SOC area was located at YC, but it contrasted to DY with abundant SOC adjacent to the dike. Relative higher SOC sediment was deposited in the southern tidal flat of CX than in the northern CX, which is proximate to the Qiantang River. The study also investigated SIC distribution in above areas and found an even distribution of SIC across most areas (Figure S1). In these areas, the SIC content was in the range of  $9\text{--}10 \text{ g kg}^{-1}$ . The highest and lowest SIC was located at YC and CX, respectively. There was an inverse trend of SOC and SIC in the southern CX.

Four general types of SOC profile were seen across the coastal region (Figure 4). The first one was a downward decreasing trend of SOC from surface to depth, and this was seen at sites DTS and CX01, which represents conditions at the surface favorable for carbon sequestration. The texture of surficial sediment gained from CX belongs to clayed silt (Table 2), and the middle and bottom part are classified as silt; this is a classic example of fine-up (upward-fining) phenomenon (Alongi, 1997). Because hydrodynamic forces promote tidal flat formation. The original flow regime was strong, and the settled coarse particles conserved less SOC. As the landward accumulation of tidal flat sediment increases, more and more fine particulates with greater SOC from adjacent vegetated marsh were deposited. The second type profile was an increasing SOC trend with depth which occurred at DY02, YC01, and YC02, which may represent sites with historically high carbon sequestration, but less currently. The SOC profile of the third type had increase SOC with depth and then at midprofile decreasing SOC with depth which indicates an area that decades ago switched from favorable conditions for carbon sequestration but recently that has declined. DY01 and YC03 were noted as this type. The fourth type was a nearly equal trend of SOC distributed in the top, intermediate, and deeper



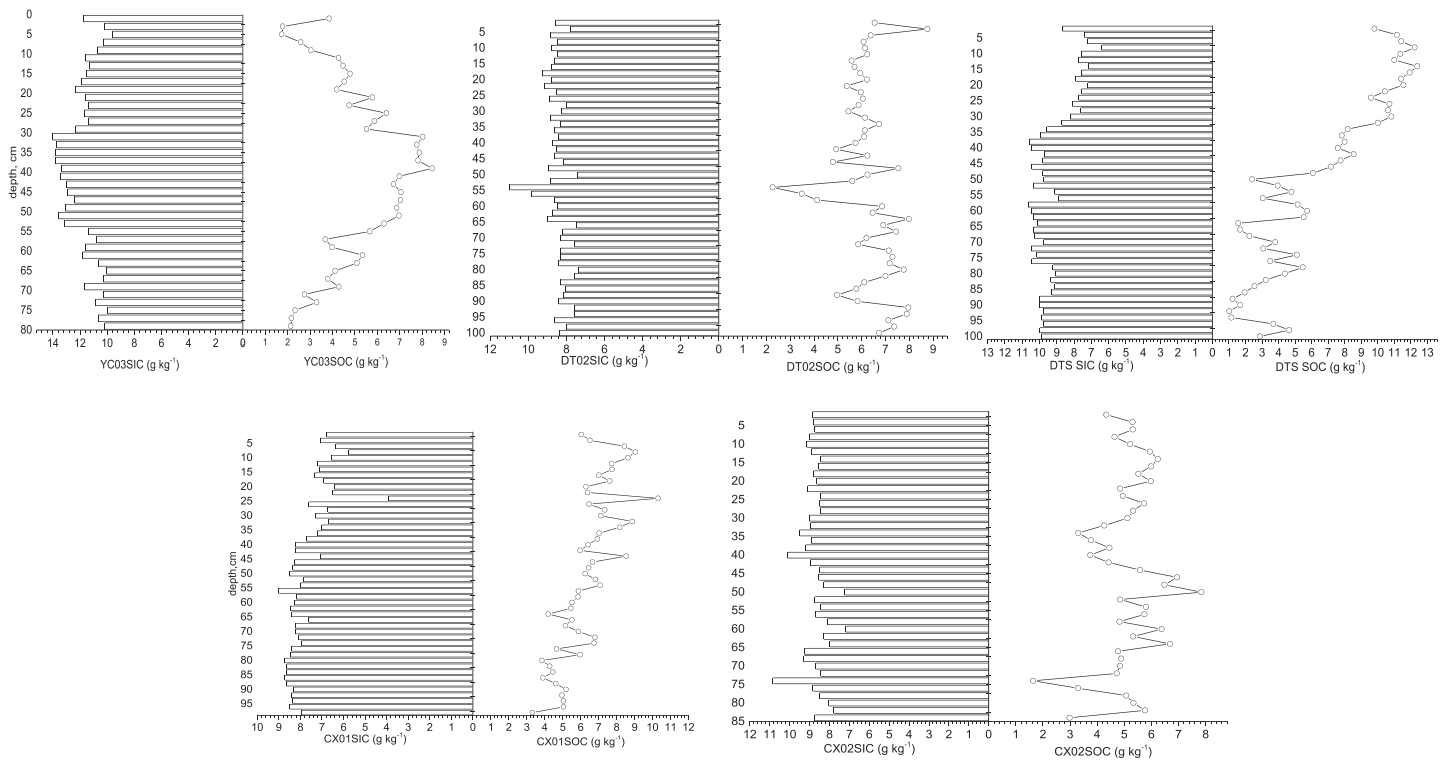


Figure 4. (continued)

**Table 2**  
Mean Sand, Silt, Clay Percent, D50, and Texture of the Study Sites

Site <sup>a</sup>	Clay	Silt	Sand	D50 (μm)	Texture (USDA)
LHS	30.08 ± 3.40	65.28 ± 2.07	4.64 ± 1.51	9.74 ± 0.56	Clayey silt
LHC	18.08 ± 8.70	77.44 ± 7.97	4.48 ± 5.42	12.73 ± 5.61	Silt
HGS	19.31 ± 13.05	80.69 ± 14.66	0.00 ± 0.16	8.95 ± 1.32	Silt
HGC	29.04 ± 11.75	69.84 ± 11.03	1.12 ± 1.95	8.51 ± 3.08	Clayey silt
DYS	11.84 ± 0.50	66.18 ± 9.14	21.97 ± 8.64	34.31 ± 7.2	Sandy silt
DYC	9.58 ± 4.48	72.99 ± 14.3	17.43 ± 17.87	34.80 ± 10.40	Sandy silt
QDS	16.69 ± 2.08	82.00 ± 2.73	1.31 ± 0.66	11.20 ± 0.64	Silt
QDC	30.20 ± 9.18	67.05 ± 6.34	2.75 ± 4.79	10.11 ± 5.54	Clayey silt
YCS	14.63 ± 1.26	81.99 ± 3.59	3.38 ± 4.60	14.19 ± 4.35	Silt
YCC	18.98 ± 6.56	74.11 ± 4.78	6.91 ± 5.24	18.01 ± 6.22	Clayey silt
DT	16.83 ± 6.24	75.06 ± 5.47	8.10 ± 7.58	20.95 ± 9.73	Silt
DTC	18.47 ± 4.07	78.78 ± 2.41	2.75 ± 2.74	16.03 ± 4.53	Silt
CXS	27.69 ± 7.50	71.90 ± 7.10	0.41 ± 0.65	10.36 ± 3.83	Clayey silt
CXC	22.14 ± 5.75	76.22 ± 4.46	1.64 ± 1.93	15.15 ± 9.34	Silt
FZS	22.39 ± 10.35	41.77 ± 5.68	35.84 ± 12.08	62.48 ± 17.02	Sand silt clay
FZC	8.14 ± 3.24	16.92 ± 5.89	74.94 ± 12.45	166.54 ± 18.54	Silty sand
JLS	40.48 ± 3.65	55.54 ± 7.66	3.98 ± 9.02	6.68 ± 8.11	Clayey silt
JLC	34.85 ± 4.83	58.72 ± 4.09	6.43 ± 4.92	8.08 ± 1.70	Clayey silt
ZJS	26.08 ± 21.88	37.49 ± 6.01	36.43 ± 27.89	37.80 ± 44.44	Sand silt clay
ZJC	21.12 ± 10.08	36.58 ± 18.55	42.29 ± 27.11	66.19 ± 59.27	Sand silt clay
DZS	6.75 ± 4.51	21.18 ± 17.69	72.07 ± 22.20	92.67 ± 29.72	Silty sand
DZC	7.07 ± 1.75	29.97 ± 8.21	62.96 ± 9.68	82.80 ± 14.62	Silty sand
YLS	6.69 ± 3.51	16.72 ± 10.84	76.68 ± 14.84	105.60 ± 15.95	Sand
YLC	20.00 ± 8.59	29.67 ± 7.37	50.32 ± 13.19	58.42 ± 25.61	Sand silt clay

<sup>a</sup>C and S represent core and surficial samples, respectively. Data are means ± SD.

sediment intervals, which indicates that conditions for C sequestration have not changed over time. HG01, HG02, and DT02 belonged to type 4.

Relatively high SOC content came from three cores (HG01, HG02, and DT02). The SOC content from HG01 and HG02 ranged from 7 to 10 g kg<sup>-1</sup>. By contrast, the SOC from the Yellow River (DY01 and DY02) was in the range of 1–2 g kg<sup>-1</sup>, the lowest among cores from two river sources. The SOC contents displayed differences in YC, as low SOC of YC01 surface (~1.5 g kg<sup>-1</sup>) and high SOC in the midplace of YC03 (7–8 g kg<sup>-1</sup>) coexisted in these places.

There were no easily discernible trends of SIC profiles in all cores except from YC02 and DTS (Figure 4), and the trend of YC02 is much more significant. The highest SIC content was found at the base of YC02. Relatively low SIC content was found in HG01, HG02, DT02, CX01, and CX01 ranging between 6 and 8 g kg<sup>-1</sup>. Slightly higher SIC content existed in DY01, DY02, YC01, YC02, YC03, and DTS; their range was between 8 and 10 g kg<sup>-1</sup>.

### 3.3. Carbon Burial in Sediments From the Northern Rivers

The sediments of LH and QD site originate from Liao River and Dagu River, which flow to Liaodong bay (north part of Bohai Sea) and Jiaozhou Bay, respectively. The study found that the mouth of Liao River had higher SOC content (at the northwest of Figure S2 LH), compared with other sites farther away the river mouth, indicating the particulate organic carbon (POC) of the suspended sediments transported by Liaohe River. The Dagu River mouth sites had lower SOC (to the west in Figure S2). Higher SOC was located at the eastern Jiaozhou Bay tidal flat. This result corresponded to high nutrient or pollution level of this area (Qingdao Municipal Marine Development Bureau, 2015). Also, the suspended sediment load of Dagu River is much lower, as indicated by low suspended particular matter in the Jiaozhou Bay (Yang et al., 2003). There was no significant difference of SOC between high tidal zone and low tidal zone in the LH and QD.

The study found the single highest SIC content in the SIC profile of LH01 (Figure 5). The burial of calcareous shell has likely contributed to the large amount of SIC. Besides the single highest SIC, the SIC content in other cores of LH did not exceed 2.2 g kg<sup>-1</sup>, contrasted with the sediments from the Yellow River and Yangtze River. No appreciable SIC was found in sediments of QD, where the small amount of SIC may relate to minimal calcareous shell accumulation. Nearly all SOC content in all profiles of QD were larger than 6 g kg<sup>-1</sup> (Figure 5). The SOC content below 50 cm did not exceed 5.5 g kg<sup>-1</sup> in all cores from LH. The SOC content of LH02 did not follow the ragged down trend pattern as other cores.

### 3.4. Carbon Burial in Sediments From the Southern Rivers

The SOC distribution pattern of FZ was similar to LH, where high SOC sediment accumulated in the river mouth (the west position of Figure S3 FZ). According to field observation, the grain size of FZ sediment deposited at Min River mouth was finer than its eastern estuary. A large area of Min River estuary is covered by silty sand with finer sediment scattered sparsely across the river estuary. This sedimentation pattern likely accounts for the extreme low SOC content in the two cores from FZ (Figure 6). The JL site contained the highest and stable surficial SOC content in the tidal flats, as its SOC content ranged within 10–15 g kg<sup>-1</sup> (Figure S3). The high SOC in JL can likely be attributed to the close proximity of sampling sites to established mangrove forest. On the other hand, the finest grain size sediment deposited in JL favors the preservation of SOC (Table 2). There appears to be no regular SOC distribution pattern seen for the ZJ site. This may partly be ascribed to complicated sand and silt sediment distribution in the Pearl River mouth (Figure S3) (Zhao, 1990). The cores of ZJ also reflected this complicated depositional history (Figure 6).

### 3.5. Carbon Burial in Sediments From Mangrove Tidal Flats

Among the two mangrove tidal flats (YL and DZ), the study found high SOC content adjacent to the river mouth in YL (the north position of Figure S4 YL), where the SOC was approaching 10 g kg<sup>-1</sup>. The mean SOC in mangrove systems proximal to river flow is much higher than those regions containing no direct river input (Breithaupt et al., 2012). The SOC from most areas of the mangrove tidal flats in DZ ranged from 3 to 4 g kg<sup>-1</sup>, and high SOC occurred in the small south area where the values ranged from 5–6 g kg<sup>-1</sup>. Contrasted with low surficial SOC, a large amount of SOC was buried below the depth of 20 cm (Figure 7). All SOC cores but DZ02 showed SOC fluctuating between 10 and 30 g kg<sup>-1</sup>. The SOC stocks in these sites were the largest among all the studied tidal flats.

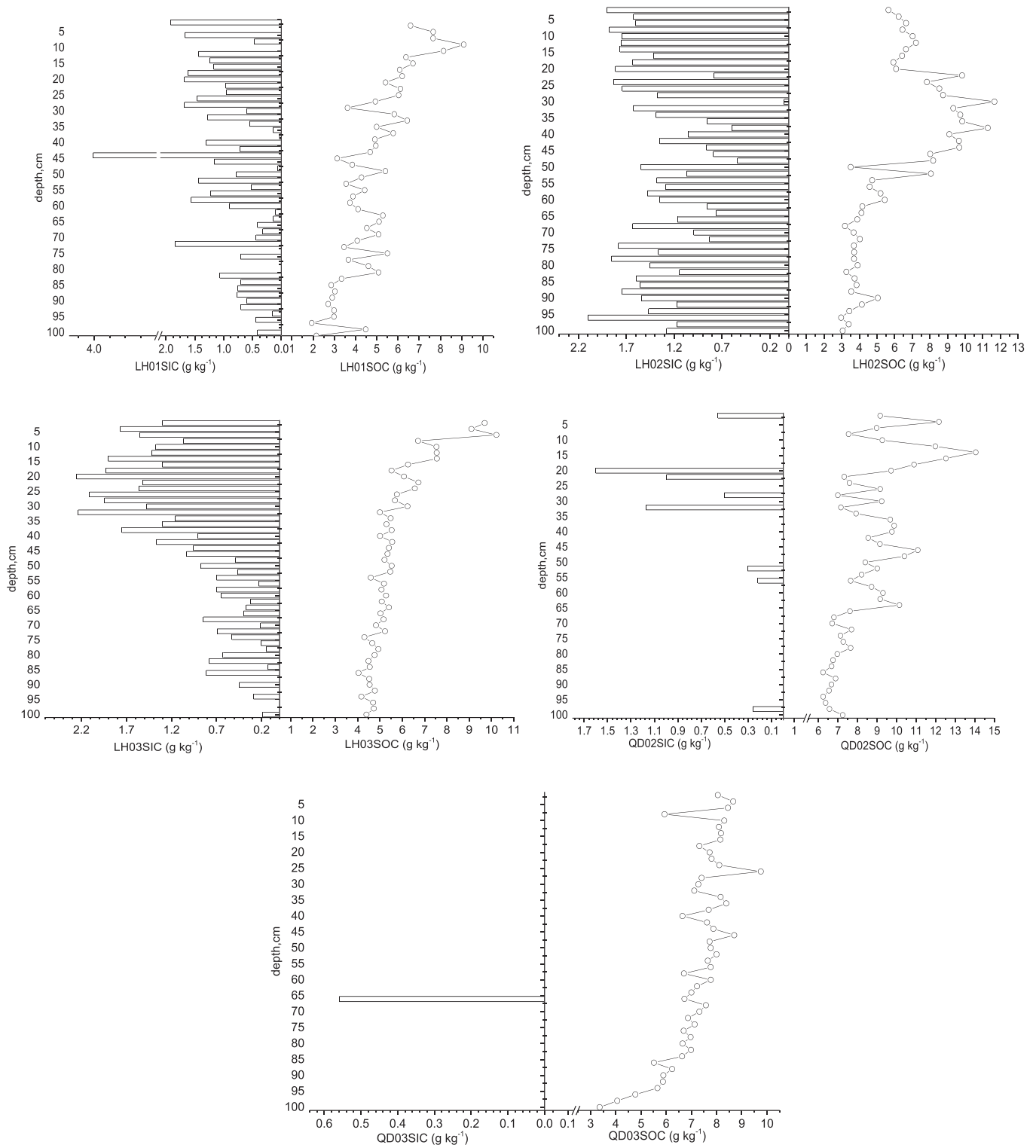
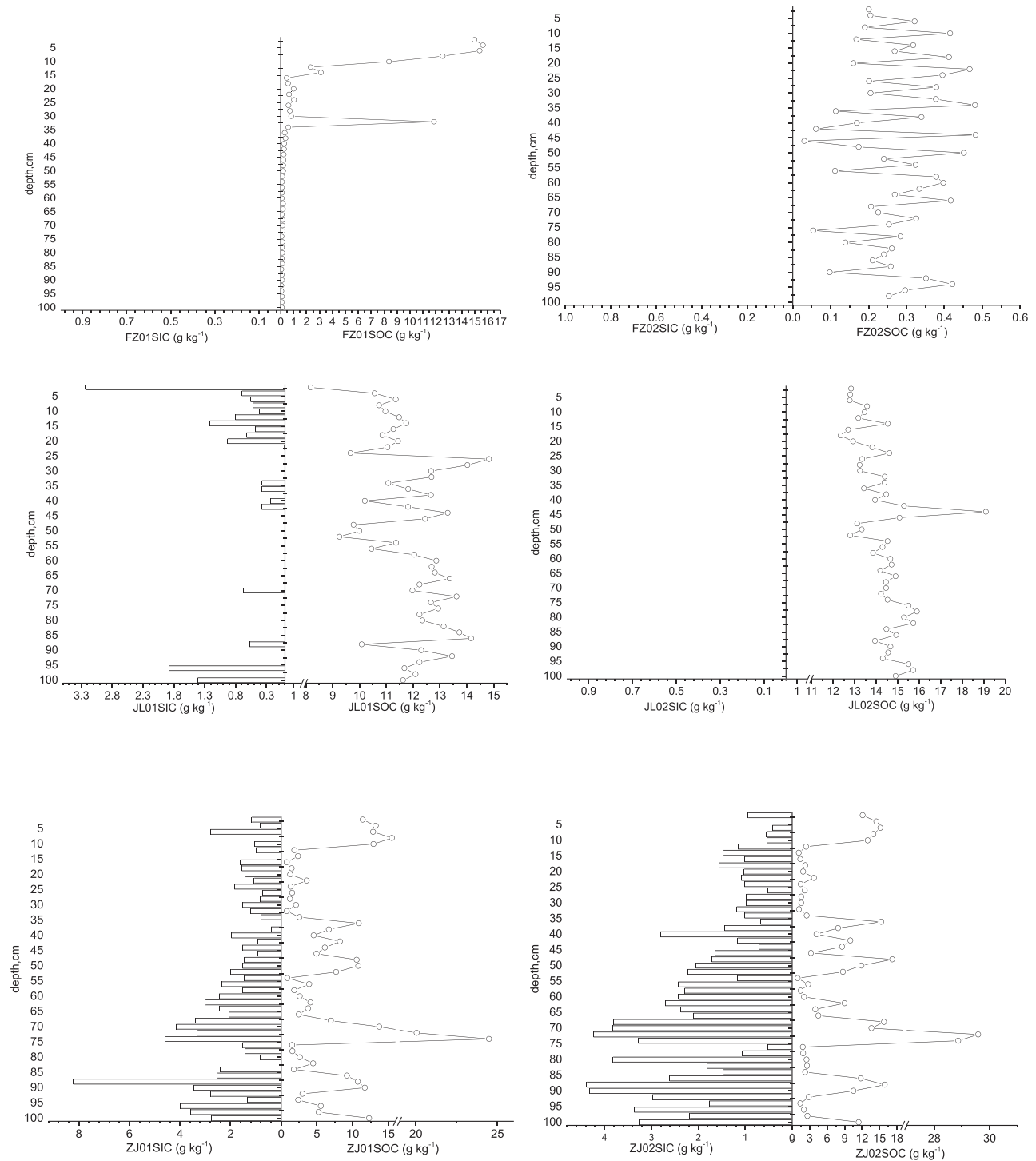


Figure 5. The SOC and SIC profiles from core samples of LH and QD.

### 3.6. Carbon Stock of Chinese Tidal Flats

The lowest carbon stock in the top 1 m was found in the Yellow River (DY) delta and Minjiang delta (FZ) (Table 3). The former was attributed to low organic carbon of suspended sediments (Wang et al., 2012), and the latter was caused by sediment size, as the reflection of extensive deposition of coarse sand in



**Figure 6.** The SOC and SIC profiles from core samples of FZ, JL, and ZJ.

Minjiang subaqueous delta (Zhen, 2000). The sites adjacent to mangrove forests, including JL, YL, and DZ, indicated highest carbon stock. Apart from these maximums and minimums, carbon stock of Chinese tidal flat ranged within 50–90 Mg C ha<sup>-1</sup> for the top 1 m of sediment (Table 3).

Based on the remote sensing methods, the study calculated the total area of Chinese tidal flat at  $1.1 \times 10^4$  km<sup>2</sup> (Table 4). The area is one half of previous study result, which was calculated by tidal range

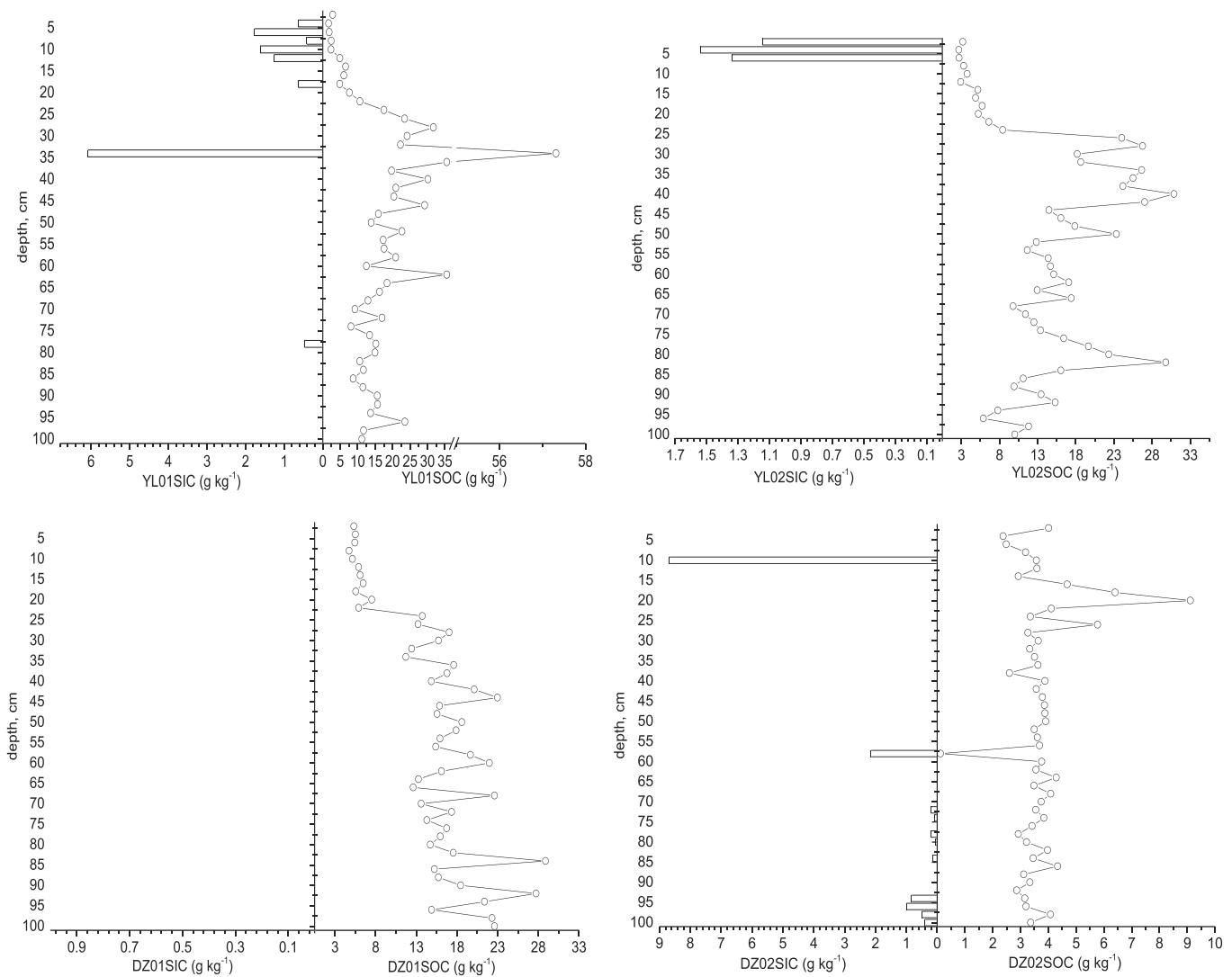


Figure 7. The SOC and SIC profiles from core samples of YL and DZ.

and bathymetry in 1980s (Chen et al., 1988; Ren, 1996). Though the specific decrease in area over the past 30 years cannot be precisely quantified due to difference in estimation methodology, a trend of substantive tidal flats loss is certain. By compiling the most recent estimations of Chinese blue carbon ecosystems, the total area of Chinese tidal area, including both vegetated (blue carbon) and nonvegetated (tidal flat), was  $1.27 \times 10^4 \text{ km}^2$  (Table 4). Therefore, 87% ( $1.1 \times 10^4 / 1.27 \times 10^4 \times 100\%$ ) of tidal area is the nonvegetated tidal flat. The total carbon stock (100 cm) of tidal flat and blue carbon ecosystem (vegetated) are 78.07 and 20.53 Tg C, respectively. Hence, nearly 80% of the carbon stock is buried in tidal flats.

## 4. Discussion

### 4.1. The Sources of Tidal Flat Sediments

Carbon burial efficiency and accumulation of organic carbon are determined by suspended sediment input and their deposition rates (Galy et al., 2007). Clay mineral composition has long been used to distinguish different sediment sources (Eisma et al., 1995). The content of illite in northern tidal flats, for example, LH, HG, DY, YC, DT, and CX, was above 55% (Table 5). The ratio of smectite to illite indicated similar sediment origin of HG and DY, or DT and CX, that is, the Yellow River (HG and DY) and Yangtze River (DT and CX). Although HG was ~150 km apart from current outlet of the Yellow River delta, the sediment transported

**Table 3**  
The SOC Stocks, Area, and Total SOC Stocks (1-m Depth) of Chinese Tidal Flats

Sites	SOC stock (Mg C ha <sup>-1</sup> )	Corresponding region <sup>a</sup>	Area (km <sup>2</sup> )	Total SOC stock (Tg C)
LH	69.9 ± 10.6	Liaoning	1,331	9.310 ± 1.417
HG	84.8 ± 1.1	Tianjin and Hebei	732	6.208 ± 0.079
DY	22.4 ± 0.6	Yellow River Delta	825	1.850 ± 0.052
QD	82.0 ± 4.4	Shandong	413	3.386 ± 0.183
YC	59.4 ± 5.2	Jiangsu	2,914	17.312 ± 1.526
DT	73.3 ± 28.9	Shanghai	378	2.769 ± 1.093
CX	67.9 ± 17.5	Zhejiang	1,328	9.014 ± 2.330
FZ	24.6 ± 3.7	Fujian (except Jiulong River Delta)	1,004	2.469 ± 0.370
JL	124.9 ± 13.1	Jiulong River Delta	219	2.741 ± 0.287
ZJ	75.1 ± 6.5	Guangdong	1,085	8.156 ± 0.710
YL	207.0 ± 26.7	Guangxi	598	12.377 ± 1.598
DZ	125.7 ± 94.8	Hainan	197	2.482 ± 1.872

<sup>a</sup>All sites but DY and JL correspond with their provinces; refer to the method to get the details.

by the Yellow River can still reach and settle at the HG site, which can be verified by both the location of chenier ridges and the historical records (Wang, 1983). The smectite/illite ratio in YC was intermediate between that in DY and DT. The coast of YC was historically influenced by the Yellow River and now also accept the sediment deposition from the Yangtze River, which is carried by the northern direction coastal currents from the Yangtze River mouth (Ren, 1986). The sediments of LH and QD originated from different local rivers. The southern tidal flats (in the south of 30°N) deposited high content of Kaolinite, which reflects the influences of humid and hot climatic conditions (Melo et al., 2001).

#### 4.2. Biogeochemical Factors Behind Different Carbon Types

The study found distinguishable inorganic carbon content in the tidal flat sediments from Yellow River (HG, DY, and YC) and Yangtze River (DT and CX). Comparatively smaller amounts of SIC, about 0.5 times smaller than the aforementioned two river sediments, was found in the ZJ cores. Among these six sites, SOC content was significantly related to SIC content in all the samples with the exception of HGSUR, HG02, and DYSUR (Figure 8). All the sediments from YC and ZJ and one of the sedi-

ments from DY showed positive relationship between SOC and SIC, while the rest indicated negative relationship between SOC and SIC (Figure 8).

Three main factors, including physicochemical characteristics of sediments at various erosion/deposition time periods, dissolution/precipitation of calcite, and growth/burial of specific phytoplankton influenced the distribution of SOC and SIC across the sites. About 90% of the sediment load of the Yellow River is derived from the Loess Plateau since 1950 (Ren & Shi, 1986). The sediment of the Yangtze River is influenced by the upper reaches, which are dominated by Paleozoic carbonate, Mesozoic detrital, and igneous rocks (Yang et al., 2004). Yang et al. (2004) demonstrated that both rivers were dominated by carbonate weathering instead of silicate weathering, but the Yangtze River experienced more intense carbonate weathering than the Yellow River. Hence, the SIC in sediments from the Yangtze River is lower than those from the Yellow River. Precambrian metamorphic rock and Quaternary fluvial sediment are distributed widely in the Pearl River basin, and 35% of the total basin area is covered by carbonates (Liu et al., 2017). The ZJ site with low SIC undergoes more intense weathering, as indicated by high kaolinite content in the sediment (Table 5).

**Table 4**  
The Comparison of Carbon Stock and Area Between Blue Carbon Ecosystem and This Study's Tidal Flats in China (1-m Depth)

Blue carbon ecosystem	Area (km <sup>2</sup> )	carbon stock (Mg C ha <sup>-1</sup> )	Total carbon stock (Tg C)	Tidal flats of this study	Area (km <sup>2</sup> )	carbon stock (Mg C ha <sup>-1</sup> )	Total carbon stock (Tg C)
Mangrove forest	228 <sup>a</sup> ; 328 <sup>b</sup> ; 345 <sup>c</sup>	270.39 <sup>d</sup>	6.165; 8.869; 9.328	The northern tidal flat <sup>e</sup>	7,921.3	65.6	49.849
Sea grass bed	109.69 <sup>f,g,h,i,j</sup>	48.3 <sup>k</sup> ; 139.7 <sup>l</sup>	0.530; 1.532	The southern tidal flat <sup>m</sup>	2,309.1	74.9	13.366
Salt marsh	1,206.54 <sup>n</sup>	64.8 <sup>o,p</sup> ; 65.2–65.8 <sup>q,r</sup> ; 82.0 <sup>s</sup>	9.668 <sup>t</sup>	Mangrove tidal flat	795.3	166.4	14.859
Total (blue carbon) <sup>u</sup>	1,661.23	—	20.53	Total (tidal flat) <sup>u</sup>	11,025	—	78.07

<sup>a</sup>Liao and Zhang (2014). <sup>b</sup>Jia (2014). <sup>c</sup>Dan et al. (2016). <sup>d</sup>Liu et al. (2014). <sup>e</sup>The tidal flats in Liaoning, Tianjin, Hebei, Shandong, Jiangsu, Shanghai and Zhejiang comprised the northern tidal flats. <sup>f</sup>Zheng et al. (2013). <sup>g</sup>Liu et al. (2016). <sup>h</sup>Zhou, Zhang, et al. (2016). <sup>i</sup>Jiang et al. (2017). <sup>j</sup>The original value was from footnote f, but newly discovered sea grass bed during 2015–2016 (footnotes g, h, and i) is added. <sup>k</sup>Li (2018). <sup>l</sup>Fourqurean et al. (2012). <sup>m</sup>The southern tidal flats scattered in Fujian, Guangdong, Guangxi, and Hainan. <sup>n</sup>Zhou, Mao, et al. (2016). <sup>o</sup>Liu et al. (2007). <sup>p</sup>The final value (0–100 cm) was the calculation result from top 20 cm SOC (l) by assuming the same of the rest 80 cm. <sup>q</sup>Gao et al. (2012). <sup>r</sup>The summed result gained from specific layers of 0- to 100-cm SOC (m). The calculation result gained from top 20-cm SOC (n) by assuming the same of the rest 80 cm. <sup>s</sup>Shao et al. (2015). <sup>t</sup>The area and stock of salt marsh in Jiangsu Province were 133 km<sup>2</sup> and 65 Mg C ha<sup>-1</sup>, respectively (Liu et al., 2004; Zhang, Shen, et al., 2005). And the stock of remainder was 82.0 Mg C ha<sup>-1</sup>. <sup>u</sup>The total area of Chinese coastal wetland, including blue carbon ecosystem and tidal flats, was 1.27 × 10<sup>4</sup> km<sup>2</sup>. Here the maximum area and carbon stock of each type of blue carbon ecosystem are chosen, due to the stable growth of the ecosystem and the strong resolution and implementation of wetland protection from local and central governments.

**Table 5**  
Average Clay Mineral Content (%) From Surficial Samples<sup>a</sup>

Site	Illite	Smectite	Kaolinite	Chlorite	S/I <sup>b</sup>
LH	58.9	14.5	13.9	12.7	0.246
HG	59.1	8.4	15.3	17.2	0.142
DY	55.3	8.3	16.1	20.3	0.150
QD	61.0	10.8	16.0	12.2	0.177
YC	58.3	7.4	15.2	19.1	0.127
DT	56.1	4.6	18.4	20.9	0.082
CX	58.8	5.1	16.3	19.8	0.087
FZ	32.8	2.2	37.9	27.1	0.067
JL	32.0	3.5	40.0	24.5	0.109
ZJ	39.5	1.3	38.4	20.8	0.033
DZ	32.6	6.4	38.7	22.3	0.196
YL	15.3	2.0	61.3	21.4	0.131

<sup>a</sup>Data provided by Qingdao Institute of Marine Geology (2016). <sup>b</sup>Ratio of smectite to illite.

The negative and positive relationship between SOC and SIC can be partly explained by the dissolution/precipitation process of calcite. The study found comparative high SOC content (>5 g kg<sup>-1</sup>) among most sites. The CO<sub>2</sub> that originated from decomposition of organic matter dissolved into water to develop carbonic acid. And carbonic acid is in equilibrium with the bicarbonate anion and hydrogen ion. This fact may inhibit the precipitation of calcite or promote the dissolution, depending on the amount of CO<sub>2</sub> produced (Müller et al., 2003). The positive relationships with relative high correlation coefficient ( $r \geq 0.6$ ) in the YC may be ascribed to high Ca<sup>2+</sup>, high pH, and relatively low SOC. A previous study showed the Ca elemental content of the Yellow River sediment was 2 times larger than the sediment from the Yangtze River, which had more dolomite than the Yellow river (Li et al., 1984). High Ca<sup>2+</sup> will promote precipitation of carbonates under high pH and carbonic acid environment.

Another factors contributing to high inorganic carbon may relate to the growth and deposition of coccolithophores. The dominant living coccolithophores of the Yellow Sea and the East China Sea are *Emiliania hux-*

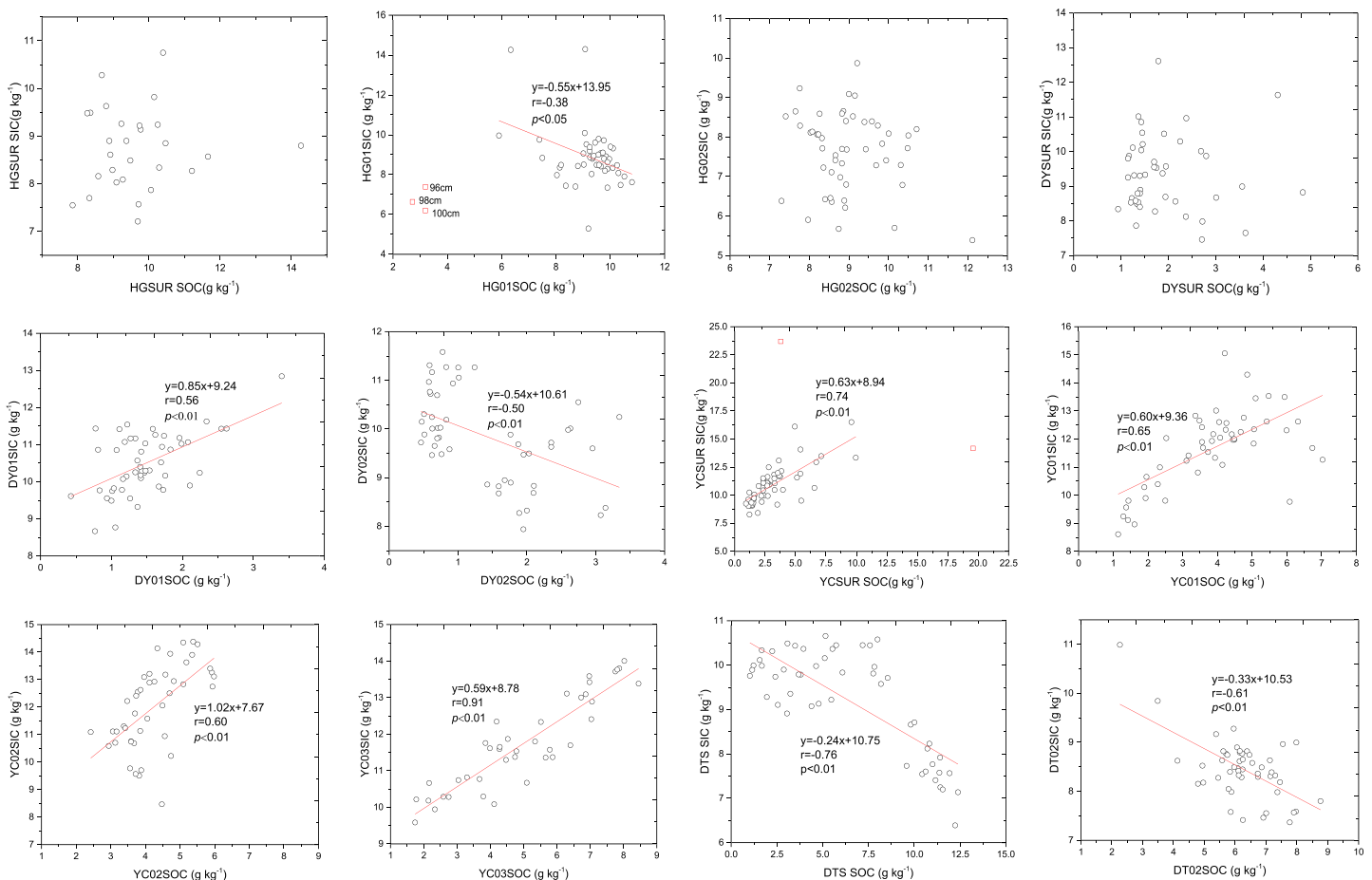


**Figure 8.** The bivariate linear correlation analysis between SOC and SIC from surficial (denoted as SUR behind site name) and core samples (denoted as number behind site name except DTS) of HG, DY, YC, DT, CX, and ZJ. Note: The several red scatters in plots of HG01 and YCSUR are deemed as extraneous variances which are eliminated from correlation analysis. There is no statistical significance between SOC and SIC from HGSUR, HG02, and DYSUR by conducting Pearson and Spearman tests.

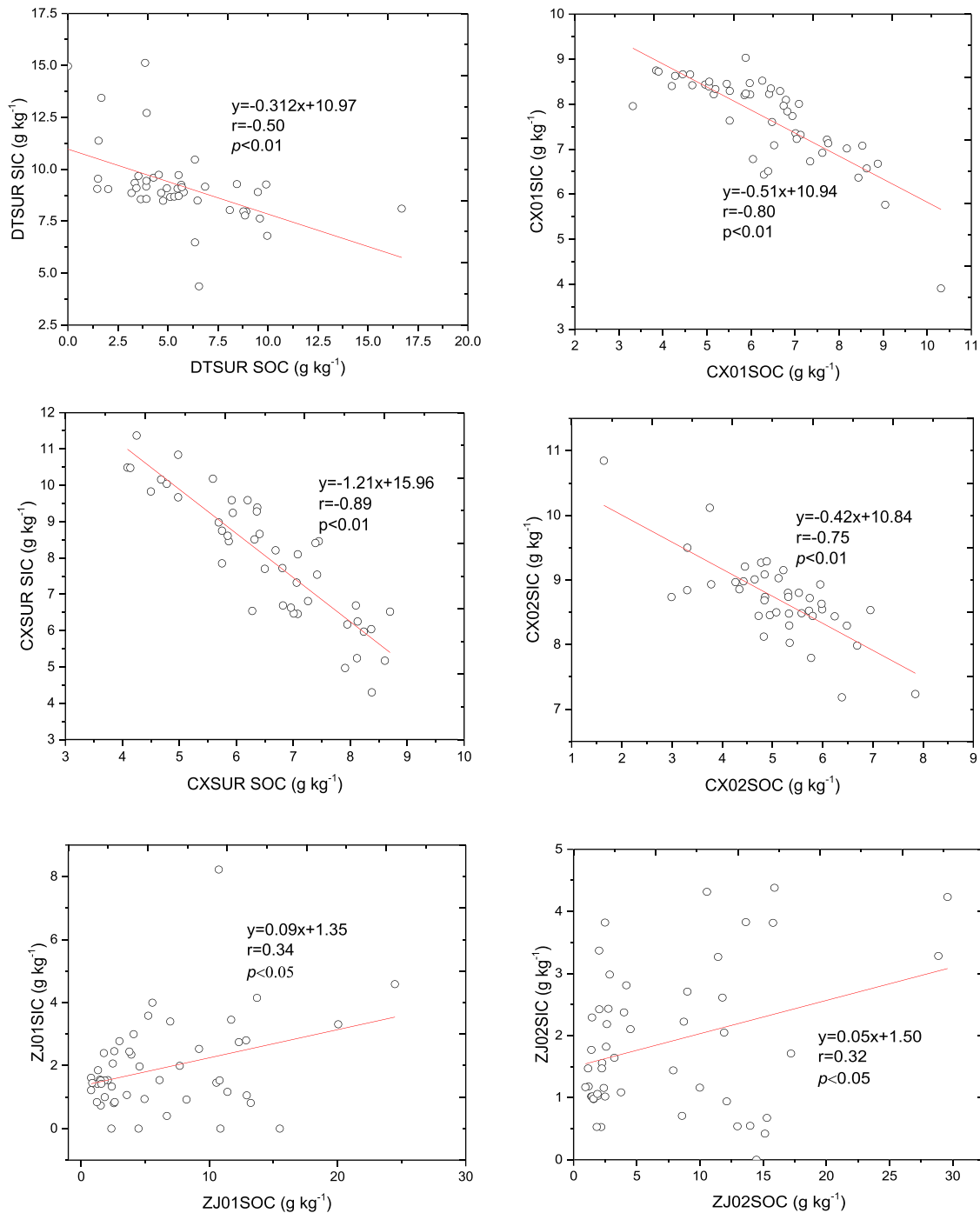


Figure 8. (continued)

*leyi* and *Gephyrocapsa oceanica*, which are also the most prominent bloom formers globally (Sun et al., 2013; Thierstein & Young, 2004). The highest surface coccoliths per milliliter was found in coastal area of Subei Shoal (adjacent to YC) in summer, while in winter, it was in the adjacent Yangtze River estuary (Sun et al., 2013). The location of highest coccolithophores corresponded to the lowest suspended sediment concentration in summer or in winter (Bian et al., 2013). This phenomenon conforms the principle that calcification of coccolithophores is predominantly a light-dependent process (Thierstein & Young, 2004). Another essential factor that controls the growth of coccolithophores is the concentration of  $\text{Ca}^{2+}$  and



**Table 6**  
*The SOC Densities of Surficial Samples*

Sampling sites <sup>a</sup>	SOC densities <sup>b</sup> (g C cm <sup>-3</sup> )	Sampling sites <sup>a</sup>	SOC densities <sup>b</sup> (g C cm <sup>-3</sup> )
LH F1	0.0083 ± 0.0012	CX F7	0.0084 ± 0.001
LH S1	0.0091 ± 0.0008	CX S7	0.0085 ± 0.0005
HG F2	0.0119 ± 0.0012	FZ F8	0.0097 ± 0.0045
HG S2	0.0123 ± 0.0006	FZ S8	0.0099 ± 0.0019
DY F3	0.0032 ± 0.0005	JL F9	0.0175 ± 0.0029
DY S3	0.0029 ± 0.0004	JL S9	0.0171 ± 0.0008
QD F4	0.0071 ± 0.0016	ZJ F10	0.0081 ± 0.0015
QD S4	0.0071 ± 0.0008	ZJ S10	0.0011 ± 0.001
YC F5	0.0052 ± 0.0018	DZ F11	0.0081 ± 0.0027
YC S5	0.0054 ± 0.0012	DZ S11	0.0059 ± 0.0005
DT F6	0.0094 ± 0.0029	YL F12	0.0032 ± 0.0008
DT S6	0.0083 ± 0.0013	YL S12	0.0047 ± 0.0011

<sup>a</sup>The sign F denotes each dry season sample and S denotes each wet season sample. For the specific code names, please refer to Figure 1.

<sup>b</sup>Mean ± SE.

higher Ca<sup>2+</sup> will promote growth (Thierstein & Young, 2004). Much more calcite is in the sediment from the Yellow River than in the sediment from the Yangtze River; the latter is enriched by Mg-containing dolomite (Li et al., 1984). Given the fact that the Ksp of calcite is two times larger than dolomite (Ball & Nordstrom, 1991), the environment of the Yellow River sediment favors the growth of coccolithophores if the suspended sediment concentration is low enough. As the sampling site YC is close to the western coastal shoal of the Yellow Sea, it seems that high surficial SIC of this area is partly impacted by the deposition of calcite calcium formed by coccolithophores. But it remains unclear how much the coccolithophores impact the SIC content since the mechanism of coccolithophores dissolution/precipitation is not fully understood (Thierstein & Young, 2004).

#### 4.3. Comparison of Carbon Density, Stock, and Sequestration Rate Between Chinese Tidal Flats and Global Coastal Area

We compiled SOC densities of all the surficial samples (Table 6) and found that carbon densities in the majority of study sites were below 0.01 g C cm<sup>-3</sup>. Only two mud tidal flats (HG and JL) had SOC densities

higher than 0.01 g C cm<sup>-3</sup>. The lowest densities occurred in the Pearl delta (ZJ) and the Yellow River delta (DY). Except these flats, the range of SOC density of Chinese tidal flats was between 0.0052 and 0.0099 g C cm<sup>-3</sup>. The average SOC density of global salt marsh was 0.039 ± 0.003 g C cm<sup>-3</sup> (Chmura et al., 2003). The SOC densities of Chinese tidal flats were much lower than the values of most coastal wetlands worldwide (Table S2). A recent study found that SOC density ranged from 0.031 to 0.044 g C m<sup>-3</sup> in the top 1 m of sediment in North American and Western European tidal marsh soil (extended data from Rogers et al., 2019). The region with the lowest SOC density, mainly located in East Asia, ranged from 0.006 to 0.008 g C m<sup>-3</sup> (extended data from Rogers et al., 2019). In our research, the SOC of the soil adjacent to mangrove areas (1–9 g kg<sup>-1</sup> in YL and DZ; 10–15 g kg<sup>-1</sup> in JL, refer to Figures S3 and S4) was much lower than SOC from no forested mangrove flats in the United States, Mexico, Australia, Brazil, and Colombia (average 36.3 g kg<sup>-1</sup>, further calculated value based on Breithaupt et al., 2012). At Chinese coast, the canopy height of 69% of Chinese mangrove forests were below 1.9 m (Donato et al., 2011; Liu et al., 2014). Sediment of smaller stature forests had lower carbon content (10–49 g kg<sup>-1</sup>) (Yang et al., 2014) than the median value of 70 g kg<sup>-1</sup> for global mangrove forests (Breithaupt et al., 2012). Apart from above fact, the surficial coarse sediments influenced the low SOC in the topsoil mangrove flats of YL and DZ, but the latter two had the most abundant carbon stock (to a 1 m depth) in the Chinese tidal flats (Table 3). If these limited mangrove flats were excluded, the carbon stock in Chinese tidal flats ranged within 22–85 Mg C ha<sup>-1</sup> (Table 3), which was lower than the mean carbon stock (0- to 100-cm depth) of tidal saline mineral soil wetlands (172 ± 15 Mg C ha<sup>-1</sup>) and organic soil wetlands (619 ± 222 Mg C ha<sup>-1</sup>) in the United States (supplementary table from Nahlik & Fennessy, 2016). The carbon stock range at Australian tidal marshes was 91–188 Mg C ha<sup>-1</sup> with a mean of 165 Mg C ha<sup>-1</sup> (Macreadie et al., 2017).

In our study, the area of Chinese tidal flats is calculated to 1.1 × 10<sup>4</sup> km<sup>2</sup>. Total carbon stock in 1-m depth of Chinese tidal flats was 78.07 Tg C. The area of tidal saline mineral soil wetland and tidal saline organic soil wetlands in the United States was 1 × 10<sup>4</sup> and 0.5 × 10<sup>4</sup> km<sup>2</sup>, and their carbon stock (0–100 cm depth) were 170 and 290 Tg C, respectively (Nahlik & Fennessy, 2016). The area and carbon stock (0- to 100-cm depth) of Australian tidal marshes were 1.38 × 10<sup>4</sup> km<sup>2</sup> and 210.98 Tg C (Macreadie et al., 2017). Meng et al. (2019) calculated 48.12–123.95 Tg C stock in the top meter of China's vegetated tidal area. We calculated that 20.53 Tg C stock was found in vegetated tidal area with decreasing salt marsh area, which is comparable to the data reported by Fu et al. (2020) (15.4 Tg C). High sedimentation rates (>1 cm yr<sup>-1</sup>, Table 1) induce high SOC burial capacity, which compensates for the lower C concentration of tidal flat sediment. This study found that 75% of Chinese tidal flats underwent greater sedimentation rates in 1990–2014 than the previous period in 1950–1990 (Table 1). This sedimentation rate change was due to rapid reclamation and sea defense wall construction after 1990, as more rapid accumulation was coincident with the establishment of new sea wall. Globally, the majority of the sediment rates were below 1 cm yr<sup>-1</sup> except for a few rivers with less

engineering projects, such as the Ganges-Brahmaputra (Table S2). So even though the SOC densities of Chinese tidal flats were much lower than planted tidal wetlands globally, the net total carbon sequestration rates were comparable to the rates of other salt marshes worldwide (Tables 1 and S2). High suspended sediment load of major rivers results in rapid sediment deposition and limits remineralization due to low oxygen availability, for example, the highest efficient carbon burial in the Bengal fan (Galy et al., 2007). The high suspended sediments of Chinese major rivers have largely contributed to the relatively high carbon sequestration in the past several decades. However, it is likely that this increasing carbon sequestration trend will not be sustained over time, given the reduced suspended sediment load and extensive coastal erosion (Cai et al., 2009; Wang et al., 2007; Yang et al., 2007).

## 5. Conclusion

Chinese tidal flats have distinct features of carbon content and stock, which are related to characteristic sediment sources and specific deposition status in the major river estuaries. The major northern tidal flat sediments, sourced from the Yellow River and the Yangtze River, had high SIC content. A positive relationship between SIC and SOC could be attributed to high  $\text{Ca}^{2+}$  and pH that promote precipitation of calcite, while high organic carbon content in DT and CX caused dissolution of carbonate, leading to a negative relationship between SIC and SOC. This study found net higher sedimentation rates in Chinese tidal flats than global coastal wetlands during the past several decades. The high sedimentation rates favor carbon sequestration. Despite much lower carbon densities in Chinese tidal flats, carbon sequestration rates are comparable to the rates of other coastal wetlands in the world. The highest carbon stock (1-m depth) was found in tidal flats adjacent to mangrove forests, which suggest trapping and sequestration of transported detrital material. The majority of Chinese coastal wetland carbon stocks are situated in the tidal flats, in which nearly 80% of carbon stock was found (78.07 Tg C). Given the reduction in suspended sediments from Chinese major rivers and increasing coastal erosion due to sea level rise, it is possible that high carbon sequestration rates will not sustain in the future.

## Data Availability Statement

The area of Chinese tidal flats is available from Murray et al. (2019a) and Murray et al. (2019b). The  $^{210}\text{Pb}$  and  $^{137}\text{Cs}$  activities are available from the data repository (<https://doi.org/10.7910/DVN/QWNLQV>). SOC from surficial and core sediments are available from the data repository (<https://doi.org/10.7910/DVN/BJLKUA>, <https://doi.org/10.7910/DVN/KIPVT4>).

## References

- Aller, R. C. (1998). Mobile deltaic and continental shelf muds as suboxic, fluidized bed reactors. *Marine Chemistry*, 61(3–4), 143–155. [https://doi.org/10.1016/S0304-4203\(98\)00024-3](https://doi.org/10.1016/S0304-4203(98)00024-3)
- Alongi, D. M. (1997). *Coastal Ecosystem Processes*. Boca Raton, FL: CRC Press.
- Appleby, P. G., & Oldfield, F. (1983). The assessment of  $^{210}\text{Pb}$  data from sites with varying sediment accumulation rates. *Hydrobiologia*, 103(1), 29–35. [https://doi.org/10.1007/978-94-009-7290-2\\_5](https://doi.org/10.1007/978-94-009-7290-2_5)
- Bai, J., Wang, J., Yan, D., Gao, H., Xiao, R., Shao, H., & Ding, Q. (2012). Spatial and temporal distributions of sediment organic carbon and total nitrogen in two marsh wetlands with different flooding frequencies of the Yellow River Delta, China. *Clean-Soil, Air, Water*, 40(10), 1137–1144. <https://dx.doi.org/10.1002/clen.201200059>
- Ball, J. W., & Nordstrom, D. K. (1991). WATEQ4F—User's manual with revised thermodynamic data base and test cases for calculating speciation of major, trace and redox elements in natural waters (No. 90–129) Virginia: United States Geological Survey.
- Bian, C., Jiang, W., Quan, Q., Wang, T., Greatbatch, R. J., & Li, W. (2013). Distributions of suspended sediment concentration in the Yellow Sea and the East China Sea based on field surveys during the four seasons of 2011. *Journal of Marine Systems*, 121–122, 24–35. <https://doi.org/10.1016/j.jmarsys.2013.03.013>
- Breithaupt, J. L., Smoak, J. M., Smith, T. J. III, Sanders, C. J., & Hoare, A. (2012). Organic carbon burial rates in mangrove sediments: Strengthening the global budget. *Global Biogeochemical Cycles*, 26, GB3011. <https://doi.org/10.1029/2012GB004375>
- Burdige, D. J. (2005). Burial of terrestrial organic matter in marine sediments: A reassessment. *Global Biogeochemical Cycles*, 19, GB4011. <https://doi.org/10.1029/2004GB002368>
- Cai, F., Su, X., Liu, J., Li, B., & Lei, G. (2009). Coastal erosion in China under the condition of global climate change and measures for its prevention. *Progress in Natural Science*, 19(4), 415–426. <https://doi.org/10.1016/j.pnsc.2008.05.034>
- Chen, J. Y., Yang, Q. L., & Zhao, C. Y. (1988). *The Survey Report About the Resources of Shanghai's Coastal Lines and Peri-Tidal Region (In Chinese)*. Shanghai: Shanghai Scientific & Technical Publishers.
- Chmura, G. L., Anisfeld, S. C., Cahoon, D. R., & Lynch, J. C. (2003). Global carbon sequestration in tidal, saline wetland soils. *Global Biogeochemical Cycles*, 17(4), 1111. <https://doi.org/10.1029/2002GB001917>
- Choi, Y., & Wang, Y. (2004). Dynamics of carbon sequestration in a coastal wetland using radiocarbon measurements. *Global Biogeochemical Cycles*, 18, GB4016. <https://doi.org/10.1029/2004GB002261>

## Acknowledgments

This study was jointly supported by Ministry of Science and Technology Project Foundation (2014FY210600), National Natural Science Foundation of China (Grant Nos. 41977321 and 41671467), Shanghai Municipal Natural Science Foundation (Grant No. ZR1412100), and the research fund from the SKLEC (2015KYYW03). The majority of lab analysis work was finished by authors in the East China Normal University. The field sampling was a collective work joined by numerous staffs from Yantai Institute of Coastal Zone Research (CAS), Qingdao Institute of Marine Geology, The First Institute of Oceanography, and East China Normal University. We sincerely thank these staffs for sample collection and custody. Without their vast enthusiasm and careful manipulation, the prodigious sampling work would not have accomplished within the scheduled time.

- Dan, X. Q., Liao, B. W., Wu, Z. B., Wu, H. J., Bao, D. M., Dan, W. Y., & Liu, S. B. (2016). Resources, conservation status and main threats of mangrove wetlands in China (in Chinese with English abstract). *Ecology and Environmental Sciences*, 2016, 25(7), 1237–1243.
- Dodla, S. K., Wang, J. J., & DeLaune, R. D. (2012). Characterization of labile organic carbon in coastal wetland soils of the Mississippi River deltaic plain: relationships to carbon functionalities. *Science of the Total Environment*, 435–436, 151–158. <https://doi.org/10.1016/j.scitotenv.2012.06.090>
- Donato, D. C., Kauffman, J. B., Murdiyarto, D., Kurnianto, S., Stidham, M., & Kanninen, M. (2011). Mangroves among the most carbon-rich forests in the tropics. *Nature Geoscience*, 4(5), 293–297. <https://doi.org/10.1038/ngeo1123>
- Duan, X. N., Wang, X. K., Fei, L., & Ouyang, Z. Y. (2008). Primary evaluation of carbon sequestration potential of wetlands in China. *Acta Ecologica Sinica*, 28(2), 463–469. [https://doi.org/10.1016/s1872-2032\(08\)60025-6](https://doi.org/10.1016/s1872-2032(08)60025-6)
- Duarte, C. M., Middelburg, J. J., & Caraco, N. (2005). Major role of marine vegetation on the oceanic carbon cycle. *Biogeosciences*, 2(1), 1–8. <https://doi.org/10.5194/bg-2-1-2005>
- Eisma, D., Ji, Z., Chen, S., Chen, M., & Van der Gaast, S. J. (1995). Clay mineral composition of recent sediments along the China Coast, in the Yellow Sea and the East China Sea. *Nioz Rapport*, 1995(4), 1–13.
- Flemming, B. W. (2002). Geographic distribution of muddy coasts. In T. Healy, Y. Wang, & J.-A. Healy (Eds.), *Muddy Coasts of the World: Processes, Deposits, and Function* (pp. 99–201). Amsterdam: Elsevier Science. [https://doi.org/10.1016/S1568-2692\(02\)80080-8](https://doi.org/10.1016/S1568-2692(02)80080-8)
- Fourqurean, J. W., Duarte, C. M., Kennedy, H., Marbà, N., Holmer, M., Mateo, M. A., et al. (2012). Seagrass ecosystems as a globally significant carbon stock. *Nature Geoscience*, 5(7), 505–509. <https://doi.org/10.1038/ngeo1477>
- Fu, C., Li, Y., Zeng, L., Zhang, H., Tu, C., Zhou, Q., et al. (2020). Stocks and losses of soil organic carbon from Chinese vegetated coastal habitats. *Global Change Biology*, gcb.15348. <https://doi.org/10.1111/gcb.15348>
- Galy, V., France-Lanord, C., Beyssac, O., Faure, P., Kudrass, H., & Palhol, F. (2007). Efficient organic carbon burial in the Bengal fan sustained by the Himalayan erosional system. *Nature*, 450(7168), 407–410. <https://doi.org/10.1038/nature06273>
- Gao, J., Bai, F., Yang, Y., Gao, S., Liu, Z., & Li, J. (2012). Influence of Spartina colonization on the supply and accumulation of organic carbon in tidal salt marshes of northern Jiangsu Province, China. *Journal of Coastal Research*, 28(2), 486–498. <https://doi.org/10.2112/jcoastres-d-11-00062.1>
- Gorma, D., Sumida, P. Y. G., Figueira, R. C. L., & Turra, A. (2020). Improving soil carbon estimates of mudflats in Araca Bay using spatial models that consider input, wave exposure and biogeochemistry. *Estuarine, Coastal and Shelf Science*, 238, 106734. <https://doi.org/10.1016/j.ecss.2020.106734>
- Gu, Y. (2004). *The Chronicle of Shanghai Municipal Farms and Land Reclamation*. Shanghai: Shanghai Academy of Social Science Press (in Chinese). Retrieved from [http://libecnu.lib.ecnu.edu.cn/record=b1607531~S0\\*chx](http://libecnu.lib.ecnu.edu.cn/record=b1607531~S0*chx)
- Hou, X., Wu, T., Hou, W., Chen, Q., Wang, Y., & Yu, L. (2016). Characteristics of coastline changes in mainland China since the early 1940s. *Science China Earth Sciences*, 59(9), 1791–1802. <https://doi.org/10.1007/s11430-016-5317-5>
- Jia, M. M. (2014). *Remote Sensing Analysis of China's Mangrove Forests Dynamics during 1973 to 2013 (Doctoral dissertation)*. Beijing: University of Chinese Academy of Sciences.
- Jiang, Z., Liu, S., Zhang, J., Zhao, C., Wu, Y., Yu, S., et al. (2017). Newly discovered seagrass beds and their potential for blue carbon in the coastal seas of Hainan Island, South China Sea. *Marine Pollution Bulletin*, 125(1–2), 513–521. <https://doi.org/10.1016/j.marpolbul.2017.07.066>
- Joshi, S. (1987). Nondestructive determination of lead-210 and radium-226 in sediments by direct photon analysis. *Journal of Radioanalytical and Nuclear Chemistry*, 116(1), 169–182. <https://dx.doi.org/10.1007/bf02037220>
- Li, M. (2018). *Carbon storage in the seagrass sediments of Guangxi, China* (Master's thesis). Guangxi normal college, Nanning.
- Li, Y. H., Hisayuki, T., Yang, T. S., & Chen, J. S. (1984). The elemental composition of suspended particles from the Yellow and Yangtze Rivers. *Geochimica et Cosmochimica Acta*, 48(7), 1561–1564. [https://doi.org/10.1016/0016-7037\(84\)90411-3](https://doi.org/10.1016/0016-7037(84)90411-3)
- Liao, B. W., & Zhang, Q. M. (2014). Area, distribution and species composition of mangrove in China (in Chinese with English abstract). *Wetland Science*, 12(4), 435–440.
- Liu, H., Huang, X. P., Wang, Y. L., Liang, Z. R., Gu, B., & Su, J. L. (2016). Newly discovered seagrass bed and its ecological characteristics in the coastal area of Caofeidian, Bohai Sea (in Chinese with English abstract). *Chinese Journal of Ecology*, 35(7), 1677–1683.
- Liu, H., Ren, H., Hui, D., Wang, W., Liao, B., & Cao, Q. (2014). Carbon stocks and potential carbon storage in the mangrove forests of China. *Journal of Environmental Management*, 133, 86–93. <https://doi.org/10.1016/j.jenvman.2013.11.037>
- Liu, J., Zhou, H., Qin, P., & Zhou, J. (2007). Effects of spartina alterniflora, salt marshes on organic carbon acquisition in intertidal zones of Jiangsu Province, China. *Ecological Engineering*, 30(3), 240–249. <https://dx.doi.org/10.1016/j.ecoleng.2007.01.010>
- Liu, Y. X., Zhang, R. S., & Li, M. C. (2004). Approach on the dynamic change and influence factors of spartina alterniflora loisel saltmarsh along the coast of the Jiangsu Province (in Chinese with English abstract). *Wetland Science*, 20(2), 18–20.
- Liu, Z., Zhao, M., Sun, H., Yang, R., Chen, B., Yang, M., et al. (2017). “Old” carbon entering the South China Sea from the carbonate-rich Pearl River Basin: Coupled action of carbonate weathering and aquatic photosynthesis. *Applied Geochemistry*, 78, 96–104. <https://dx.doi.org/10.1016/j.apgeochem.2016.12.014>
- Ma, Z., Melville, D. S., Liu, J., Chen, Y., Yang, H., Ren, W., et al. (2014). Rethinking China's new great wall. *Science*, 346(6212), 912–914. <https://dx.doi.org/10.1126/science.1257258>
- Macreadie, P. I., Ollivier, Q. R., Kelleway, J. J., Serrano, O., Carnell, P. E., Ewers Lewis, C. J., et al. (2017). Carbon sequestration by Australian tidal marshes. *Scientific Reports*, 7, 44,071. <https://doi.org/10.1038/srep44071>
- McLeod, E., Chmura, G. L., Bouillon, S., Salm, R., Björk, M., Duarte, C. M., et al. (2011). A blueprint for blue carbon: toward an improved understanding of the role of vegetated coastal habitats in sequestering CO<sub>2</sub>. *Frontiers in Ecology and the Environment*, 9(10), 552–560. <https://doi.org/10.1890/110004>
- Melo, V. F., Singh, B., Schaefer, C. E. G. R., Novais, R. F., & Fontes, M. P. F. (2001). Chemical and mineralogical properties of kaolinite-rich Brazilian soils. *Soil Science Society of America Journal*, 65(4), 1324–1333. <https://doi.org/10.2136/sssaj2001.6541324x>
- Meng, W., Feagin, R. A., Hu, B., He, M., & Li, H. (2019). The spatial distribution of blue carbon in the coastal wetlands of China. *Estuarine, Coastal and Shelf Science*, 222, 13–20. <https://doi.org/10.1016/j.ecss.2019.03.010>
- Mi, N. A., Wang, S., Liu, J., Yu, G., Zhang, W., & Jobbagy, E. (2008). Soil inorganic carbon storage pattern in China. *Global Change Biology*, 14(10), 2380–2387. <https://doi.org/10.1111/j.1365-2486.2008.01642.x>
- Ministry of Water Resources Pearl River Water Resources Commission (1994). *The Annals of Pearl River (in Chinese)*. Guangzhou, China: Guangdong Technology Publishing House.
- Ministry of Water Resources Songliao River Water Resources Commission (2002). *The annals of Liao River (in Chinese)*. Changchun: Jilin People's Publishing House.

- Müller, B., Wang, Y., Dittrich, M., & Wehrli, B. (2003). Influence of organic carbon decomposition on calcite dissolution in surficial sediments of a freshwater lake. *Water Research*, 37(18), 4524–4532. [https://doi.org/10.1016/S0043-1354\(03\)00381-6](https://doi.org/10.1016/S0043-1354(03)00381-6)
- Murray, N. J., Phinn, S. R., DeWitt, M., Ferrari, R., Johnston, R., Lyons, M. B., et al. (2019a). The global distribution and trajectory of tidal flats. *Nature*, 565(7738), 222–225. <https://doi.org/10.1038/s41586-018-0805-8>
- Murray, N. J., Phinn, S. R., DeWitt, M., Ferrari, R., Johnston, R., Lyons, M. B., et al. (2019b). Murray global intertidal change classification. ee. ImageCollection("UQ/murray/Intertidal/v1\_1/global\_intertidal"). Retrieved from [https://developers.google.com/earth-engine/datasets/catalog/UQ\\_murray\\_Intertidal\\_v1\\_1\\_global\\_intertidal](https://developers.google.com/earth-engine/datasets/catalog/UQ_murray_Intertidal_v1_1_global_intertidal)
- Nahlik, A. M., & Fennessy, M. S. (2016). Carbon storage in US wetlands. *Nature Communications*, 7, 13,835. <https://doi.org/10.1038/ncomms13835>
- Nellemann, C., Corcoran, E., Duarte, C. M., Valdes, L., DeYoung, C., Fonseca, L., & Grimsditch, G. (2009). Blue Carbon. *A Rapid Response Assessment* (p. 80). Birkeland Trykkeri AS, Birkeland, Norway: U. N. Environment Programme, GRID-Arendal.
- Nelson, D. W., & Sommers, L. E. (1996). Total carbon, organic carbon, and organic matter. In D. L. Sparks, A. L. Page, P. A. Helmke, & R. H. Loeppert (Eds.), *Methods of Soil Analysis, Part 3. Chemical Methods*. (Book Series no. 5 (pp. 996–997). Madison: WI: ASA. and SSSA. <https://doi.org/10.2136/sssabookser5.3>
- Nriagu, J. O. (1978). *The Biogeochemistry of Lead in the Environment*. Amsterdam: Elsevier North-Holland Biomedical Press.
- Paulson Institute, the Convention on Wetlands Management office (PRC), IGSNRR (CAS) & Lao Niu Foundation (2015). Blueprint of coastal wetland conservation and management in China. Paulson Institute. <http://www.paulsoninstitute.org/wp-content/uploads/2016/08/Wetland-Report-EN-Final.pdf>
- Perillo, G. M., Wolanski, E., Cahoon, D. R., & Brinson, M. M. (2009). *Coastal Wetlands: An Integrated Ecosystem Approach*. Amsterdam: Elsevier.
- Postma, H. (1981). Exchange of materials between the North Sea and the Wadden Sea. *Marine Geology*, 40(1–2), 199–213. [https://doi.org/10.1016/0025-3227\(81\)90050-5](https://doi.org/10.1016/0025-3227(81)90050-5)
- Qingdao Municipal Marine Development Bureau (2015). Qingdao marine environment annual report 2014. Retrieved from <http://ocean.qingdao.gov.cn/n12479801/n32205288/160125182106067781.html> (in Chinese)
- Ramsar Convention Secretariat (Ed) (2013). *The Ramsar Convention Manual: A Guide to the Convention on Wetlands* (sixth ed.). Gland: Ramsar Convention Secretariat.
- Ren, M. E. (1986). *The Investigation Report About Natural Sources of Coastline and Tidal Flats in Jiangsu Province*. (in Chinese. Beijing: China Ocean Press.
- Ren, M. E. (1996). The current status and strategy of Chinese tidal mudflats (in Chinese without English abstract). *Bulletin of the Chinese Academy of Sciences*, 6, 440–443.
- Ren, M. E., & Shi, Y. L. (1986). Sediment discharge of the Yellow River (China) and its effect on the sedimentation of the Bohai and the Yellow Sea. *Continental Shelf Research*, 6(6), 785–810. [https://dx.doi.org/10.1016/0278-4343\(86\)90037-3](https://dx.doi.org/10.1016/0278-4343(86)90037-3)
- Roberts, H. H., DeLaune, R. D., White, J. R., Li, C., Sasser, C. E., Braud, D., et al. (2015). Floods and cold front passages: Impacts on coastal marshes in a river diversion setting (Wax Lake Delta, Louisiana). *Journal of Coastal Research*, 31(5), 1057–1068. <https://doi.org/10.2112/JCOASTRES-D-14-00173.1>
- Rogers, K., Kelleway, J. J., Saintilan, N., Megonigal, J. P., Adams, J. B., Holmquist, J. R., et al. (2019). Wetland carbon storage controlled by millennial-scale variation in relative sea-level rise. *Nature*, 567(7746), 91–95. <https://doi.org/10.1038/s41586-019-0951-7>
- Shao, X., Yang, W., & Wu, M. (2015). Seasonal dynamics of soil labile organic carbon and enzyme activities in relation to vegetation types in Hangzhou Bay tidal flat wetland. *PLoS ONE*, 10(11), e0142677. <https://doi.org/10.1371/journal.pone.0142677>
- Sun, J., Gu, X. Y., Feng, Y., Jin, S. F., Jiang, W., Jin, H., & Chen, J. (2013). Summer and winter living coccolithophores in the Yellow Sea and the East China Sea. *Biogeosciences*, 11(3), 779–806. <https://doi.org/10.5194/bg-11-779-2014>
- Thierstein, H. R., & Young, J. R. (2004). *Coccolithophores: From Molecular Processes to Global Impact*. Berlin Heidelberg, New York: Springer-Verlag. <https://doi.org/10.1007/978-3-662-06278-4>
- Volkman, J. K., Rohjans, D., Rullkötter, J., Scholz-Böttcher, B. M., & Liebezeit, G. (2000). Sources and diagenesis of organic matter in tidal flat sediments from the German Wadden Sea. *Continental Shelf Research*, 20(10–11), 1139–1158. [https://doi.org/10.1016/S0278-4343\(00\)00016-9](https://doi.org/10.1016/S0278-4343(00)00016-9)
- Wang, H., Yang, Z., Saito, Y., Liu, J. P., Sun, X., & Wang, Y. (2007). Stepwise decreases of the Huanghe (Yellow River) sediment load (1950–2005): Impacts of climate change and human activities. *Global and Planetary Change*, 57(3–4), 331–354. <https://doi.org/10.1016/j.gloplacha.2007.01.003>
- Wang, S., Fu, B., Piao, S., Lü, Y., Ciais, P., Feng, X., & Wang, Y. (2016). Reduced sediment transport in the Yellow River due to anthropogenic changes. *Nature Geoscience*, 9(1), 38–41. <https://doi.org/10.1038/ngeo2602>
- Wang, X., Ma, H., Li, R., Song, Z., & Wu, J. (2012). Seasonal fluxes and source variation of organic carbon transported by two major Chinese Rivers: The Yellow River and Changjiang (Yangtze) River. *Global Biogeochemical Cycles*, 26, GB2025. <https://doi.org/10.1029/2011GB004130>
- Wang, Y. (1983). The mudflat system of China. *Canadian Journal of Fisheries and Aquatic Sciences*, 40(S1), s160–s171. <https://doi.org/10.1139/f83-278>
- Wang, Y., Healy, T., & Member of SCOR Working Group 106 (2002). Definition, properties, and classification of muddy coasts. In T. Healy, Y. Wang, & J.-A. Healy (Eds.), *Muddy Coasts of the World: Processes, Deposits, and Function* (pp. 9–18). Amsterdam: Elsevier Science. [https://doi.org/10.1016/S1568-2692\(02\)80076-6](https://doi.org/10.1016/S1568-2692(02)80076-6)
- West, T. O., & Post, W. M. (2002). Soil organic carbon sequestration rates by tillage and crop rotation. *Soil Science Society of America Journal*, 66(6), 1930–1946. <https://doi.org/10.2136/sssaj2002.1930>
- Xu, K., & Milliman, J. D. (2009). Seasonal variations of sediment discharge from the Yangtze River before and after impoundment of the Three Gorges Dam. *Geomorphology*, 104(3–4), 276–283. <https://doi.org/10.1016/j.geomorph.2008.09.004>
- Yang, J., Gao, J., Liu, B., & Zhang, W. (2014). Sediment deposits and organic carbon sequestration along mangrove coasts of the Leizhou Peninsula, southern China. *Estuarine, Coastal and Shelf Science*, 136, 3–10. <https://doi.org/10.1016/j.ecss.2013.11.020>
- Yang, S., Jung, H., & Li, C. (2004). Two unique weathering regimes in the Changjiang and Huanghe drainage basins: Geochemical evidence from river sediments. *Sedimentary Geology*, 164(1–2), 19–34. <https://doi.org/10.1016/j.sedgeo.2003.08.001>
- Yang, S. L., Meng, Y., Zhang, J., Xue, Y. Z., Wei, H., Chen, H. T., et al. (2003). The characteristics of suspended particulate matter and its response to hydrodynamic forces and pollutant emission in the Jiaozhou Bay. *Chinese Science Bulletin*, 48(23), 2493–2498.
- Yang, S. L., Zhang, J., Dai, S. B., Li, M., & Xu, X. J. (2007). Effect of deposition and erosion within the main river channel and large lakes on sediment delivery to the estuary of the Yangtze River. *Journal of Geophysical Research*, 112, F02005. <https://doi.org/10.1029/2006JF000484>

- Zhang, H.-G., Guo, Y. X., Huang, W. G., & Zhou, C. B. (2005). A remote sensing investigation of inning and silting in Hangzhou bay since 1986 (in Chinese with English abstract). *Remote Sensing for Land & Resources*, 17(2), 50–54.
- Zhang, R. S., Shen, Y. M., Lu, L. Y., Yan, S. G., Wang, Y. H., Li, J. L., & Zhang, Z. L. (2005). Formation of spartina alterniflora salt marsh on Jiangsu coast, China (in Chinese with English abstract). *Oceanologia Et Limnologia Sinica*, 36(4), 358–366.
- Zhang, Y., Ding, W., Luo, J., & Donnison, A. (2010). Changes in sediment organic carbon dynamics in an Eastern Chinese coastal wetland following invasion by a C<sub>4</sub> plant *Spartina alterniflora*. *Soil Biology and Biochemistry*, 42(10), 1712–1720. <https://dx.doi.org/10.1016/j.soilbio.2010.06.006>
- Zhao, H. T. (1990). *The Evolution of the Pearl River Mouth*. (in Chinese. Beijing: China Ocean Press.
- Zhen, Z. F. (2000). *Formation and Evolution of Underwater Delta in Minjiang Estuary (Master's thesis)*. Xiamen: Third Institute of Oceanography.
- Zheng, F. Y., Qiu, G. L., Fan, H. Q., & Zhang, W. (2013). Diversity, distribution and conservation of Chinese seagrass species (in Chinese with English abstract). *Biodiversity Science*, 21(5), 517–526. <https://doi.org/10.3724/SP.J.1003.2013.10038>
- Zhou, C. H., Mao, Q. Y., Xu, X., Fang, C. M., Luo, Y. M., & Li, B. (2016). Preliminary analysis of C sequestration potential of blue carbon ecosystems on Chinese coastal zone (in Chinese with English abstract). *Scientia Sinica Vitae*, 46(4), 475–486.
- Zhou, Y., Zhang, X. M., Xu, S. C., Song, X. Y., Lin, H. Y., Wang, P. M., & Gu, R. T. (2016). New discovery of larger seagrass beds with areas > 50 ha in temperate waters of China: An unusual large seagrass (*Zostera japonica*) bed in the Yellow River estuary (in Chinese with English abstract). *Marine Sciences*, 2016, 40(9), 95–97.